BEYOND CONSERVATISM: DIFFUSION POLICIES IN OFFLINE MULTI-AGENT REINFORCEMENT LEARNING

Anonymous authors
Paper under double-blind review

ABSTRACT

We present a novel Diffusion Offline Multi-agent Model (DOM2) for offline Multi-Agent Reinforcement Learning (MARL). Different from existing algorithms that rely mainly on conservatism in policy design, DOM2 enhances policy expressiveness and diversity based on diffusion model. Specifically, we incorporate a diffusion model into the policy network and propose a trajectory-based data-augmentation scheme in training. These key ingredients make our algorithm more robust to environment changes and achieve significant improvements in performance, generalization and data-efficiency. Our extensive experimental results demonstrate that DOM2 outperforms existing state-of-the-art methods in all multi-agent particle and multi-agent MuJoCo environments, and generalizes significantly better to shifted environments (in 28 out of 30 settings evaluated) thanks to its high expressiveness and diversity. Moreover, DOM2 is ultra data efficient and requires no more than 5% data for achieving the same performance compared to existing algorithms (a $20\times$ improvement in data efficiency).

1 INTRODUCTION

Offline reinforcement learning (RL), commonly referred to as batch RL, aims to learn efficient policies exclusively from previously gathered data without interacting with the environment (Lange et al., 2012; Levine et al., 2020). Since the agent has to sample the data from a fixed dataset, naive offline RL approaches fail to learn policies for out-of-distribution actions or states (Wu et al., 2019; Kumar et al., 2019), and the obtained Q-value estimation for these actions will be inaccurate with unpredictable consequences. Recent progress in tackling the problem focuses on *conservatism* by introducing regularization terms for policy and Q-value training (Fujimoto et al., 2019; Kumar et al., 2020a; Fujimoto & Gu, 2021; Kostrikov et al., 2021a; Lee et al., 2022). These conservatism-based offline RL algorithms have achieved significant progress in difficult offline multi-agent reinforcement learning settings (MARL) (Jiang & Lu, 2021; Yang et al., 2021; Pan et al., 2022).

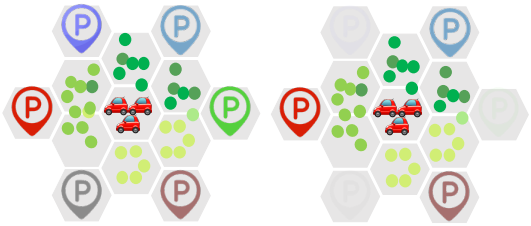

Figure 1: Standard environment (Left) and shifted environment dismissing 3 landmarks randomly (right).

Despite the potential benefits, existing methods have limitations in several aspects. Firstly, the design of the policy network and the corresponding regularizer limits the expressiveness and diversity due to conservatism. Consequently, the resulting policy may be suboptimal and fail to represent complex strategies, e.g., policies with multi-modal distribution over actions (Kumar et al., 2019; Wang et al., 2022). Secondly, in multi-agent scenarios, the conservatism-based method is prone to getting trapped in poor local optima. This occurs when each agent is incentivized to maximize its own reward without efficient cooperation with other agents in existing algorithms (Yang et al., 2021; Pan et al., 2022). To demonstrate this phenomenon, we conduct experiment on a simple MARL scenario consisting of 3 agents and 6 landmarks (Figure 1), to highlight the importance of policy expressiveness and diversity in MARL. In this scenario, the agents are asked to cover 3 landmarks and are rewarded based on their proximity to the nearest landmark while being penalized for collisions. We first train the agents with 6 target landmarks and then randomly dismiss 3 of them in evaluation. Our experiments demonstrate that existing methods (MA-CQL and OMAR (Pan et al., 2022)), which

constrain policies through regularization, limit the expressiveness of each agent and hinder the ability of the agents to cooperate with diversity. As a result, only limited solutions are found. Therefore, in order to design robust algorithms with good generalization capabilities, it is crucial to develop methods beyond conservatism for better performance and more efficient cooperation among agents.

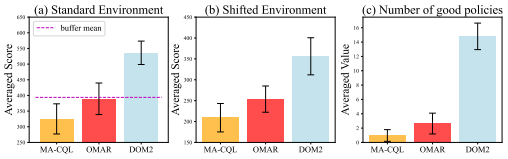

Figure 2: Results in different environments. For experimental details, see Appendix C.4.

To boost the policy expressiveness and diversity, we propose a novel algorithm based on *diffusion* for the offline multi-agent setting, called Diffusion Offline Multi-Agent Model (DOM2). Diffusion model has shown significant success in generating data with high quality and diversity (Ho et al., 2020; Song et al., 2020b; Wang et al., 2022; Croitoru et al., 2023). Our goal is to leverage this advantage to promote expressiveness and diversity of the policy. Specifically, the policy for each agent is built using the accelerated DPM-solver to sample actions (Lu et al., 2022). In order to train an appropriate policy that performs well, we propose a trajectory-based data-augmentation method to facilitate policy training by efficient data sampling. These techniques enable the policy to generate solutions with high quality and diversity, and overcome the limitations of conservatism-based approaches. Figure 2 shows that in the 3-agent example, DOM2 can find a more diverse set of solutions with high performance and generalization, compared to conservatism-based methods such as MA-CQL and OMAR (Pan et al., 2022). Our contributions are summarized as follows.

- We propose a novel Diffusion Offline Multi-Agent Model (DOM2) algorithm to address the limitations of conservatism-based methods. DOM2 is a decentralized training and execution framework consisting of three critical components: diffusion-based policy with an accelerated solver (sampling within 10 steps), appropriate policy regularizer, and a trajectory-based data augmentation method for enhancing learning.
- We conduct extensive numerical experiments on Multi-agent Particles Environments (MPE) and Multi-agent MuJoCo (MAMuJoCo) HalfCheetah environments. Our results show that DOM2 achieves significantly better performance improvement over state-of-the-art methods in all tasks.
- We show that DOM2 possesses much better generalization abilities and outperforms existing methods in shifted environments, i.e., DOM2 achieves state-of-the-art performance in 17 out of 18 MPE shifted settings and 11 out of 12 MAMuJoCo shifted settings. Moreover, DOM2 is ultra-data-efficient and achieves SOTA performance with $20\times$ times less data.

2 Related Work

Due to space limitation, we discuss a set of most related work here. In Appendix A, we provide a more comprehensive discussion of related results.

Offline RL and MARL: In offline RL, designing proper regularizers is a critical method to address the distribution shift, e.g., BRAC (Wu et al., 2019), BEAR (Kumar et al., 2019), BCQ (Fujimoto et al., 2019) and TD3+BC (Fujimoto & Gu, 2021) purposed novel policy regularizers, and CQL (Kumar et al., 2020a), IQL (Kostrikov et al., 2021b) and TD3-CVAE (Rezaeifar et al., 2022) developed new Q-value regularizers. Several recent work has achieved success in offline MARL, e.g., MA-BCQ (Jiang & Lu, 2021), MA-ICQ (Yang et al., 2021) and OMAR (Pan et al., 2022).

Diffusion models: Being a powerful generative model, the diffusion model has demonstrated its great strength in generation quality and diversity (Ho et al., 2020; Song et al., 2020b;a). Most existing results on diffusion has focused on accelerating sampling efficiently (Lu et al., 2022; Bao et al., 2022). Recently, there have been works attempting to incorporate diffusion into offline RL and offline MARL, including Diffusion-QL (Wang et al., 2022), SfBC (Chen et al., 2022) and IDQL (Hansen-Estruch et al., 2023) in single-agent RL and MA-DIFF (Zhu et al., 2023) in MARL.

We note that most existing works focus on conservatism for algorithm design. Our algorithm goes beyond this and focuses on introducing diffusion into offline MARL with the accelerated solver under fully decentralized training and execution structure.

3 BACKGROUND

In this section, we introduce the offline multi-agent reinforcement learning problem and provide preliminaries for the diffusion probabilistic model as the background for our proposed algorithm.

Offline Multi-Agent Reinforcement Learning. A fully cooperative multi-agent task can be modeled as a decentralized partially observable Markov decision process (Dec-POMDP (Oliehoek & Amato, 2016)) with n agents consisting of a tuple $G = \langle \mathcal{I}, \mathcal{S}, \mathcal{O}, \mathcal{A}, \Pi, \mathcal{P}, \mathcal{R}, n, \gamma \rangle$. Here $\mathcal{I}$ is the set of agents, $\mathcal{S}$ is the global state space, $\mathcal{O} = (\mathcal{O}_1, ..., \mathcal{O}_n)$ is the set of observations with $\mathcal{O}_n$ being the set of observation for agent n. $\mathcal{A} = (\mathcal{A}_1, ..., \mathcal{A}_n)$ is the set of actions for the agents ($\mathcal{A}_n$ is the set of actions for agent n), $\Pi = (\Pi_1, ..., \Pi_n)$ is the set of policies, and $\mathcal{P}$ is the function class of the transition probability $\mathcal{S} \times \mathcal{A} \times \mathcal{S}' \to [0, 1]$. At each time step t, each agent chooses an action $a_j^t \in \mathcal{A}_j$ based on the policy $\pi_j \in \Pi_j$ and historical observation $o_j^{t-1} \in \mathcal{O}_j$. The next state is determined by the transition probability $P \in \mathcal{P}$. Each agent then receives a reward $r_j^t \in \mathcal{R} : \mathcal{S} \times \mathcal{A} \to \mathbb{R}$ and a private observation $o_j^t \in \mathcal{O}_i$. The goal of the agents is to find the optimal policies $\boldsymbol{\pi} = (\pi_1, ..., \pi_n)$ such that each agent can maximize the discounted return: $\mathbb{E}[\sum_{t=0}^{\infty} \gamma^t r_j^t]$ (the joint discounted return is $\mathbb{E}[\sum_{j=1}^{n} \sum_{t=0}^{\infty} \gamma^t r_j^t]$), where γ is the discount factor. Offline reinforcement learning requires that the data to train the agents is sampled from a given dataset $\mathcal{D}$ generated from some potentially unknown behavior policy $\boldsymbol{\pi_\beta}$ (which can be arbitrary). This means that the procedure for training agents is separated from the interaction with environments.

Conservative Q-Learning. For training the critic in offline RL, the conservative Q-Learning (CQL) method (Kumar et al., 2020a) is to train the Q-value function $Q_{\boldsymbol{\phi}}(\boldsymbol{o}, \boldsymbol{a})$ parameterized by $\boldsymbol{\phi}$, by minimizing the temporal difference (TD) loss plus the conservative regularizer. Specifically, the objective to optimize the Q-value for each agent j is given by:

$$\begin{aligned} \mathcal{L}(\boldsymbol{\phi}_j) = \mathbb{E}_{(\boldsymbol{o}_j, \boldsymbol{a}_j) \sim \mathcal{D}_j}[(r_j + \gamma \min_{k=1,2} \overline{Q}_{\overline{\boldsymbol{\phi}}_j}^k(\boldsymbol{o}_j', \overline{\pi}_j(\boldsymbol{o}_j')) - Q_{\boldsymbol{\phi}_j}(\boldsymbol{o}_j, \boldsymbol{a}_j))^2] \\ + \zeta \mathbb{E}_{(\boldsymbol{o}_j, \boldsymbol{a}_j) \sim \mathcal{D}_j}[\log \sum_{\tilde{\boldsymbol{a}}_j} \exp(Q_{\boldsymbol{\phi}_j}(\boldsymbol{o}_j, \tilde{\boldsymbol{a}}_j)) - Q_{\boldsymbol{\phi}_j}(\boldsymbol{o}_j, \boldsymbol{a}_j)]. \end{aligned} \tag{1}$$

The first term is the TD error to minimize the Bellman operator with the double Q-learning trick (Fujimoto et al., 2019; Hasselt, 2010; Lillicrap et al., 2015), where $\overline{Q}_{\overline{\boldsymbol{\phi}}_j}, \overline{\pi}_j$ denotes the target network and $\boldsymbol{o}_j'$ is the next observation for agent j after taking action $\boldsymbol{a}_j$. The second term is a conservative regularizer, where $\tilde{\boldsymbol{a}}_j$ is a random action uniformly sampled in the action space and ζ is a hyperparameter to balance two terms. The regularizer is to address the extrapolation error by encouraging large Q-values and penalizing low Q-values for state-action pairs in the dataset.

Diffusion Probabilistic Model. We present a high-level introduction to the Diffusion Probabilistic Model (DPM) (Sohl-Dickstein et al., 2015; Song et al., 2020b; Ho et al., 2020) (detailed introduction is in Appendix B). DPM is a deep generative model that learns the unknown data distribution $\boldsymbol{x}_0 \sim q_0(\boldsymbol{x}_0)$ from the dataset. DPM has a predefined forward noising process characterized by a stochastic differential equation (SDE) $\mathrm{d}\boldsymbol{x}_t = f(t)\boldsymbol{x}_t \mathrm{d}t + g(t)\mathrm{d}\boldsymbol{w}_t$ (Equation (5) in Song et al. (2020b)) and a trainable reverse denoising process characterized by the SDE $\mathrm{d}\boldsymbol{x}_t = [f(t)\boldsymbol{x}_t - g^2(t)\nabla_{\boldsymbol{x}_t} \log q_t(\boldsymbol{x}_t)]\mathrm{d}t + g(t)\mathrm{d}\overline{\boldsymbol{w}}_t$ (Equation (6) in Song et al. (2020b)) shown in Figure 3. Here $\boldsymbol{w}_t, \overline{\boldsymbol{w}}_t$ are standard Brownian motions, $f(t), g(t)$ are predefined functions such that $q_{0t}(\boldsymbol{x}_t|\boldsymbol{x}_0) = \mathcal{N}(\boldsymbol{x}_t; \alpha_t \boldsymbol{x}_0, \sigma_t^2 \boldsymbol{I})$ for some constant $\alpha_t, \sigma_t > 0$ and $q_T(\boldsymbol{x}_T) \approx \mathcal{N}(\boldsymbol{x}_T; \boldsymbol{0}, \tilde{\sigma}^2 \boldsymbol{I})$ is almost a Gaussian distribution for constant $\tilde{\sigma} > 0$. However, there exists an unknown term $\nabla_{\boldsymbol{x}_t} \log q_t(\boldsymbol{x}_t)$, which is called the *score function* (Song et al., 2020a). In order to generate data close to the distribution $q_0(\boldsymbol{x}_0)$ by the reverse SDE, DPM defines a score-based model $\boldsymbol{\epsilon}_{\boldsymbol{\theta}}(\boldsymbol{x}_t, t)$ to learn the score function and optimize parameter $\boldsymbol{\theta}$ such that $\boldsymbol{\theta}^* = \arg\min_{\boldsymbol{\theta}} \mathbb{E}_{\boldsymbol{x}_0 \sim q_0(\boldsymbol{x}_0), \boldsymbol{\epsilon} \sim \mathcal{N}(\boldsymbol{0}, \boldsymbol{I}), t \sim \mathcal{U}(0,T)}[\|\epsilon - \boldsymbol{\epsilon}_{\boldsymbol{\theta}}(\alpha_t \boldsymbol{x}_0 + \sigma_t \boldsymbol{\epsilon}, t)\|_2^2]$ ($\mathcal{U}(0, T)$ is the uniform distribution in $[0, T]$, same later). With the learned score function, we can sample data by discretizing the reverse SDE. To enable faster sampling, DPM-solver (Lu et al., 2022) provides an efficiently

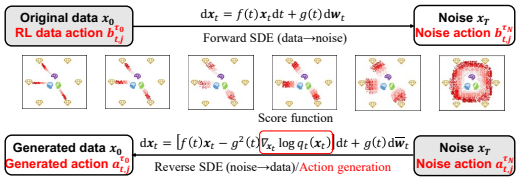

Figure 3: Diffusion probabilistic model as a stochastic differential equation (SDE) (Song et al., 2020b) and relationship with Offline MARL.

faster sampling method and the first-order iterative equation (Equation (3.7) in Lu et al. (2022)) to denoise is given by $\boldsymbol{x}_{t_i} = \frac{\alpha_{t_i}}{\alpha_{t_{i-1}}}\boldsymbol{x}_{t_{i-1}} - \sigma_{t_i}(\frac{\alpha_{t_i}\sigma_{t_{i-1}}}{\alpha_{t_{i-1}}\sigma_{t_i}} - 1)\boldsymbol{\epsilon}_{\boldsymbol{\theta}}(\boldsymbol{x}_{t_{i-1}}, t_{i-1})$.

In Figure 3, we highlight a crucial message that we can efficiently incorporate the procedure of data generation into offline MARL as the action generator. Intuitively, we can utilize the fixed dataset to learn an action generator by noising the sampled actions in the dataset, and then denoising it inversely. The procedure assembles data generation in the diffusion model. However, it is important to note that there is a critical difference between the objectives of diffusion and RL. Specifically, in diffusion model, the goal is to generate data with a distribution close to the distribution of the training dataset, whereas in offline MARL, one hopes to find actions (policies) that maximize the joint discounted return. This difference influences the design of the action generator. Properly handling it is the key in our design, which will be detailed below in Section 4.

4 Proposed Method

In this section, we present the DOM2 algorithm shown in Figure 4. In the following, we first discuss how we generate the actions with diffusion in Section 4.1. Next, we show how to design appropriate objective functions in policy learning in Section 4.2. We then present the data augmentation method in Section 4.3. Finally, we present the whole procedure of DOM2 in Section 4.4.

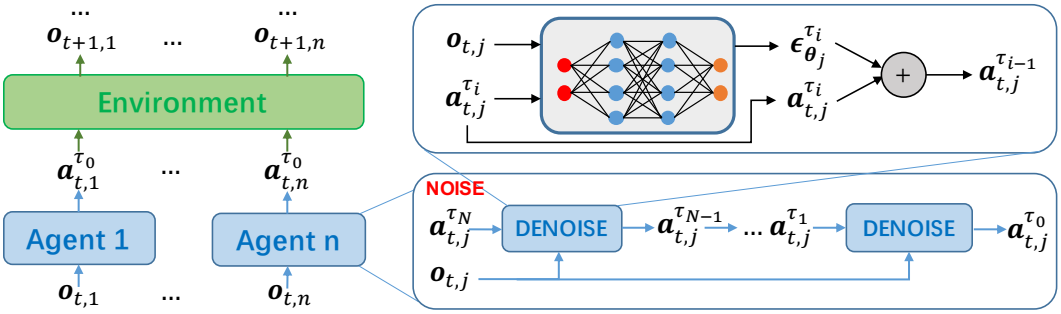

Figure 4: Diagram of the DOM2 algorithm. Each agent generates actions with diffusion.

4.1 Diffusion in Offline MARL

We first present the diffusion component in DOM2, which generates actions by denoising a Gaussian noise iteratively (shown on the right side of Figure 4). Denote the timestep indices in an episode by $\{t\}_{t=1}^{T}$, the diffusion step indices by $\tau \in [\tau_0, \tau_N]$, and the agent by $\{j\}_{j=1}^{n}$. Below, to facilitate understanding, we introduce the diffusion idea in continuous time, based on Song et al. (2020b); Lu et al. (2022). We then present our algorithm design by specifying the discrete DPM-solver-based steps (Lu et al., 2022) and discretizing diffusion timesteps, i.e., from $[\tau_0, \tau_N]$ to $\{\tau_i\}_{i=0}^{N}$.

(**Noising**) Noising the action in diffusion is modeled as a forward process from τ_0 to τ_N. Specifically, we start with the collected action data at τ_0, denoted by $\boldsymbol{b}_{t,j}^{\tau_0} \sim \boldsymbol{\pi}_{\boldsymbol{\beta}_j}(\cdot|\boldsymbol{o}_{t,j})$, which is collected from the behavior policy $\boldsymbol{\pi}_{\boldsymbol{\beta}_j}(\cdot|\boldsymbol{o}_{t,j})$. We then perform a set of noising operations on intermediate data $\{\boldsymbol{b}_{t,j}^{\tau}\}_{\tau\in[\tau_0,\tau_N]}$, and eventually generate $\boldsymbol{b}_{t,j}^{\tau_N}$, which (ideally) is close to Gaussian noise at τ_N. This forward process satisfies that for $\forall \tau \in [\tau_0, \tau_N]$, the transition probability $q_{\tau_0\tau}(\boldsymbol{b}_{t,j}^{\tau}|\boldsymbol{b}_{t,j}^{\tau_0}) = \mathcal{N}(\boldsymbol{b}_{t,j}^{\tau}; \alpha_\tau \boldsymbol{b}_{t,j}^{\tau_0}, \sigma_\tau^2 \boldsymbol{I})$ (Lu et al., 2022). The selection of the noise schedules α_τ, σ_τ enables that $q_{\tau_N}(\boldsymbol{b}_{t,j}^{\tau_N}|\boldsymbol{o}_{t,j}) \approx \mathcal{N}(\boldsymbol{b}_{t,j}^{\tau_N}; \boldsymbol{0}, \tilde{\sigma}^2\boldsymbol{I})$ for some $\tilde{\sigma} > 0$, which is almost a Gaussian noise. According to Song et al. (2020b); Kingma et al. (2021), there exists a corresponding reverse process of SDE from τ_N to τ_0 (based on Equation (2.4) in Lu et al. (2022)) considering $\boldsymbol{o}_{t,j}$ as conditions:

$$\mathrm{d}\boldsymbol{a}_{t,j}^{\tau} = [f(\tau)\boldsymbol{a}_{t,j}^{\tau} - g^2(\tau)\underbrace{\nabla_{\boldsymbol{b}_{t,j}^{\tau}} q_\tau(\boldsymbol{b}_{t,j}^{\tau}|\boldsymbol{o}_{t,j})}_{\text{Neural Network } \boldsymbol{\epsilon}_{\boldsymbol{\theta}_j}}]\mathrm{d}\tau + g(\tau)\mathrm{d}\overline{\boldsymbol{w}}_\tau, \boldsymbol{a}_{t,j}^{\tau_N} \sim q_{\tau_N}(\boldsymbol{b}_{t,j}^{\tau_N}|\boldsymbol{o}_{t,j}), \tag{2}$$

where $f(\tau) = \frac{\mathrm{d}\log\alpha_\tau}{\mathrm{d}\tau}, g^2(\tau) = \frac{\mathrm{d}\sigma_\tau^2}{\mathrm{d}\tau} - 2\frac{\mathrm{d}\log\alpha_\tau}{\mathrm{d}\tau}\sigma_\tau^2$ and $\overline{\boldsymbol{w}}_t$ is a standard Brownion motion, and $\boldsymbol{a}_{t,j}^{\tau_0}$ is the generated action for agent j at time t. To fully determine the reverse process of SDE described by Equation 2, we need the access to the scaled conditional *score function* $-\sigma_\tau \nabla_{\boldsymbol{b}_{t,j}^{\tau}} q_\tau(\boldsymbol{b}_{t,j}^{\tau}|\boldsymbol{o}_{t,j})$ at

each τ. We use a neural network $\boldsymbol{\epsilon}_{\boldsymbol{\theta}_j}(\boldsymbol{b}^{\tau}_{t,j}, \boldsymbol{o}_{t,j}, \tau)$ to represent it and the architecture is the multiple-layered residual network, which is shown in Figure 8 that resembles U-Net (Ho et al., 2020; Chen et al., 2022). The objective of optimizing the parameter $\boldsymbol{\theta}_j$ is (based on Lu et al. (2022)):

$$\mathcal{L}_{bc}(\boldsymbol{\theta}_j) = \mathbb{E}_{(\boldsymbol{o}_{t,j}, \boldsymbol{a}^{\tau_0}_{t,j}) \sim \mathcal{D}_j, \boldsymbol{\epsilon} \sim \mathcal{N}(\mathbf{0}, \boldsymbol{I}), \tau \in \mathcal{U}(\{\tau_i\}_{i=0}^{N})}[\|\boldsymbol{\epsilon} - \boldsymbol{\epsilon}_{\boldsymbol{\theta}_j}(\alpha_\tau \boldsymbol{a}^{\tau_0}_{t,j} + \sigma_\tau \boldsymbol{\epsilon}, \boldsymbol{o}_{t,j}, \tau)\|_2^2]. \tag{3}$$

(**Denoising**) After training the neural network $\boldsymbol{\epsilon}_{\boldsymbol{\theta}_j}$, we can then generate the actions by solving the diffusion SDE in Equation 2 (plugging in $-\boldsymbol{\epsilon}_{\boldsymbol{\theta}_j}(\boldsymbol{a}^{\tau}_{t,j}, \boldsymbol{o}_{t,j}, \tau)/\sigma_\tau$ to replace the true score function $\nabla_{\boldsymbol{b}^{\tau}_{t,j}} \log q_\tau(\boldsymbol{b}^{\boldsymbol{\tau}}_{\boldsymbol{t,j}} | \boldsymbol{o}_{t,j})$). Here we evolve the reverse process of SDE from $\boldsymbol{a}^{\tau_N}_{t,j} \sim \mathcal{N}(\boldsymbol{a}^{\tau_N}_{t,j}; \mathbf{0}, \boldsymbol{I})$, a Gaussian noise, and we take $\boldsymbol{a}^{\tau_0}_{t,j}$ as the final action. To facilitate faster sampling, we discretize the reverse process of SDE in $[\tau_0, \tau_N]$ into $N+1$ diffusion timesteps $\{\tau_i\}_{i=0}^{N}$ (the partition details are shown in Appendix B) and adopt the first-order DPM-solver-based method (Equation (3.7) in Lu et al. (2022)) to iteratively denoise from $\boldsymbol{a}^{\tau_N}_{t,j} \sim \mathcal{N}(\boldsymbol{a}^{\tau_N}_{t,j}; \mathbf{0}, \boldsymbol{I})$ to $\boldsymbol{a}^{\tau_0}_{t,j}$ for $i = N, ..., 1$ written as:

$$\boldsymbol{a}^{\tau_{i-1}}_{t,j} = \frac{\alpha_{\tau_{i-1}}}{\alpha_{\tau_i}} \boldsymbol{a}^{\tau_i}_{t,j} - \sigma_{\tau_i} \left(\frac{\alpha_{\tau_i} \sigma_{\tau_{i-1}}}{\alpha_{\tau_{i-1}} \sigma_{\tau_i}} - 1 \right) \boldsymbol{\epsilon}_{\boldsymbol{\theta}_j}(\boldsymbol{a}^{\tau_i}_{t,j}, \boldsymbol{o}_{t,j}, \tau_i) \text{ for } i = N, ...1, \tag{4}$$

and such iterative denoising steps are corresponding to the diagram in the right side of Figure 4.

4.2 Policy Improvement

Notice that only optimizing $\boldsymbol{\theta}_j$ by Equation 3 is not sufficient in offline MARL, because the generated actions will only be close to the behavior policy under diffusion. To achieve policy improvement, we follow Wang et al. (2022) to involve the Q-value and use the following loss function:

$$\mathcal{L}(\boldsymbol{\theta}_j) = \mathcal{L}_{bc}(\boldsymbol{\theta}_j) + \mathcal{L}_q(\boldsymbol{\theta}_j) = \mathcal{L}_{bc}(\boldsymbol{\theta}_j) - \tilde{\eta} \mathbb{E}_{(\boldsymbol{o}_j, \boldsymbol{a}_j) \sim \mathcal{D}_j, \boldsymbol{a}_j^{\tau_0} \sim \pi_{\boldsymbol{\theta}_j}}[Q_{\boldsymbol{\phi}_j}(\boldsymbol{o}_j, \boldsymbol{a}_j^{\tau_0})]. \tag{5}$$

The second term $\mathcal{L}_q(\boldsymbol{\theta}_j)$ is called Q-loss (Wang et al., 2022) for policy improvement , where $\boldsymbol{a}_j^{\tau_0}$ is generated by Equation 4, $\boldsymbol{\phi}_j$ is the network parameter of Q-value function for agent j, $\tilde{\eta} = \frac{\eta}{\mathbb{E}_{(\boldsymbol{s}_j, \boldsymbol{a}_j) \sim \mathcal{D}}[Q_{\boldsymbol{\phi}_j}(\boldsymbol{o}_j, \boldsymbol{a}_j)]}$ and η is a hyperparameter. This Q-value is normalized to control the scale of Q-value functions (Fujimoto & Gu, 2021) and η is used to balance the weights. The combination of two terms ensures that the policy can preferentially sample actions with high values. The reason is that the policy trained by optimizing Equation 5 can generate actions with different distributions compared to the behavior policy, and the policy prefers to sample actions with higher Q-values (corresponding to better performance). To train efficient Q-values for policy improvement, we optimize Equation 1 as the objective (Kumar et al., 2020a).

4.3 Data Augmentation

In DOM2, in addition to the novel policy design with its training objectives, we also introduce a data-augmentation method to scale up the size of the dataset (shown in Algorithm 1). Specifically, we replicate trajectories $\mathcal{T}_i \in \mathcal{D}$ with high return values (i.e., with the return value, denoted by $Return(\mathcal{T}_i)$, higher than threshold values) in the dataset. Specifically, we define a set of threshold values $\mathcal{R} = \{r_{\text{th},1}, ..., r_{\text{th},K}\}$. Then, we compare the reward of each trajectory with every threshold value and replicate the trajectory once whenever its return is higher than the compared threshold (Line 4), such that trajectories with higher returns can replicate more times. Doing so allows us to create more data efficiently and improve the performance of the policy by increasing the probability of sampling trajectories with better performance in the dataset. We emphasize that our method is different from the data augmented works, where the objective is to use a diffusion model as a data generator for downstream tasks, e.g., Trabucco et al. (2023); Lu et al. (2023b). Our method is designed to enhance the offline dataset for facilitating diffusion-based policy and Q-value training in offline MARL.

Algorithm 1 Data `Augmentation`

1: **Input:** Dataset $\mathcal{D}$ with trajectories $\{\mathcal{T}_i\}_{i=1}^{L}$.
2: $\mathcal{D}' \leftarrow \mathcal{D}$
3: **for** every $r_{\text{th}} \in \mathcal{R}$ **do**
4: $\quad \mathcal{D}' \leftarrow \mathcal{D}' + \{\mathcal{T}_i \in \mathcal{D} | Return(\mathcal{T}_i) \geq r_{\text{th}}\}$.
5: **end for**
6: **Return:** Augmented dataset $\mathcal{D}'$.

4.4 The DOM2 Algorithm

The resulting DOM2 algorithm is presented in Algorithm 2. Line 1 is the initialization step. Line 2 is the data-augmentation step. Line 5 is the sampling procedure for the preparation of the mini-batch data from the augmented dataset to train the agents. Lines 6 and 7 are the update of actor and

critic parameters, i.e., the policy and the Q-value. Line 8 is the soft update procedure for the target networks. Our algorithm provides a systematic way to integrate diffusion into RL algorithm with appropriate regularizers and how to train the diffusion policy in a decentralized multi-agent setting.

Algorithm 2 Diffusion Offline Multi-agent Model (DOM2) Algorithm

1: **Input:** Initialize Q-networks $Q^1_{\boldsymbol{\phi}_j}, Q^2_{\boldsymbol{\phi}_j}$, policy network π_j with random parameters $\boldsymbol{\phi}^1_j, \boldsymbol{\phi}^2_j, \boldsymbol{\theta}_j$, target networks with $\overline{\boldsymbol{\phi}}^1_j \leftarrow \boldsymbol{\phi}^1_j, \overline{\boldsymbol{\phi}}^2_j \leftarrow \boldsymbol{\phi}^2_j, \overline{\boldsymbol{\theta}}_j \leftarrow \boldsymbol{\theta}_j$ for each agent $j = 1, \ldots, N$ and dataset $\mathcal{D}$. // Initialization
2: Run $\mathcal{D}' = \texttt{Augmentation}(\mathcal{D})$ to generate an augmented dataset $\mathcal{D}'$. // Data Augmentation
3: **for** training step $t = 1$ **to** T **do**
4: **for** agent $j = 1$ **to** n **do**
5: Sample a random minibatch of $\mathcal{S}$ samples$(\boldsymbol{o}_j, \boldsymbol{a}_j, \boldsymbol{r}_j, \boldsymbol{o}'_j)$ from dataset $\mathcal{D}'$. // Sampling
6: Update critics $\boldsymbol{\phi}^1_j, \boldsymbol{\phi}^2_j$ to minimize Equation 1. // Update Critic
7: Update the actor $\boldsymbol{\theta}_j$ to minimize Equation 5. // Update Actor with Diffusion
8: Update target networks: $\overline{\boldsymbol{\phi}}^k_j \leftarrow \rho\boldsymbol{\phi}^k_j + (1-\rho)\overline{\boldsymbol{\phi}}^k_j, (k = 1, 2), \overline{\boldsymbol{\theta}}_j \leftarrow \rho\boldsymbol{\theta}_j + (1-\rho)\overline{\boldsymbol{\theta}}_j$.
9: **end for**
10: **end for**

Some comparisons with the recent diffusion-based methods for action generation are in place. First of all, we use the diffusion policy in the multi-agent setting. Then, different from Diffuser (Janner et al., 2022), our method generates actions independently among different timesteps, while Diffuser generates a sequence of actions as a trajectory in the episode using a combination of diffusion model and the transformer architecture, so the actions are dependent among different timesteps. Compared to the DDPM-based diffusion policy (Wang et al., 2022), we use the first-order DPM-Solver (Lu et al., 2022) and the multi-layer residual network as the noise network (Chen et al., 2022) for better and faster action sampling, while the DDPM-based diffusion policy (Wang et al., 2022) uses the multi-layer perceptron (MLP) to learn score functions. In contrast to SfBC (Chen et al., 2022), we use the conservative Q-value for policy improvement to learn the score functions, while SfBC only uses the BC loss in the procedure. Unlike MA-DIFF (Zhu et al., 2023) that uses an attention-based diffusion model in centralized training and centralized or decentralized execution, our method is decentralized in both the training and execution procedure. Below, we will demonstrate, with extensive experiments, that our DOM2 method achieves superior performance, significant generalization, and data efficiency compared to the state-of-the-art offline MARL algorithms.

5 Experiments

We evaluate our method in different multi-agent environments and datasets. We focus on three primary metrics, performance (how is DOM2 compared to other SOTA baselines), generalization (can DOM2 generalize well if the environment configurations change), and data efficiency (is our algorithm applicable with small datasets and low-quality datasets).

5.1 Experiment Setup

Environments: We conduct experiments in two widely-used multi-agent tasks including the multi-agent particle environments (MPE) (Lowe et al., 2017) and high-dimensional and challenging multi-agent MuJoCo (MAMuJoCo) tasks (Peng et al., 2021). In MPE, agents known as physical particles need to cooperate with each other to solve the tasks. The MAMuJoCo is an extension for MuJoCo locomotion tasks to enable the robot to run with the cooperation of agents. We use the Predator-prey, World, Cooperative navigation in MPE and 2-agent HalfCheetah in MAMuJoCo as the experimental environments. The details are shown in Appendix C.1. To demonstrate the generalization capability of our DOM2 algorithm, we conduct experiments in both standard environments and shifted environments. Compared to the standard environments, the features of the environments are changed randomly to increase the difficulty for the agent to finish the task, which will be shown later.

Datasets: We construct 6 different datasets following Fu et al. (2020) to represent different qualities of behavior policies: random, random-medium, medium-replay, medium, medium-expert and expert dataset. The construction details are shown in Appendix C.3

Baseline: We compare the DOM2 algorithm with the following state-of-the-art baseline offline MARL algorithms: MA-CQL (Jiang & Lu, 2021), OMAR (Pan et al., 2022), MA-SfBC as the

extension of the single agent diffusion-based policy SfBC (Chen et al., 2022) and MA-DIFF (Zhu et al., 2023). Our methods are all built on the independent TD3 with decentralized actors and critics. Each algorithm is executed for 5 random seeds and the mean performance and the standard deviation are presented. A detailed description of hyperparameters, neural network structures, and setup can be found in Appendix C.2.

5.2 MULTI-AGENT PARTICLE ENVIRONMENT

Performace. Table 1 shows the mean episode returns (same for Table 2 to 4 below) of the algorithms under different datasets. We see that in all settings, DOM2 significantly outperforms MA-CQL, OMAR, and MA-SfBC. We also observe that DOM2 has smaller deviations in most settings compared to other algorithms, demonstrating that DOM2 is more stable in different environments.

Table 1: Performance comparison of DOM2 with MA-CQL, OMAR, and MA-SfBC.

Predator Prey	MA-CQL	OMAR	MA-SfBC	DOM2
Random	1.0±7.6	14.3±9.5	3.5±2.5	**208.7±57.3**
Random Medium	1.7±13.0	67.7±30.8	12.0±10.7	**133.0±39.9**
Medium Replay	35.0±21.6	86.8±43.7	26.1±10.0	**150.5±23.9**
Medium	101.0±42.5	116.9± 45.2	127.0±50.9	**155.8±48.1**
Medium Expert	113.2±36.7	128.3±35.2	152.3±41.2	**184.4±25.3**
Expert	140.9±33.3	202.8±27.1	256.0±26.9	**259.1±22.8**
World	MA-CQL	OMAR	MA-SfBC	DOM2
Random	-3.8±3.0	0.0±3.3	-1.8±1.9	**40.0±14.3**
Random Medium	-6.6±1.1	28.7±10.4	4.0±5.5	**42.7±9.3**
Medium Replay	15.9±14.2	21.1±15.6	9.1±5.9	**65.9±10.6**
Medium	44.3±14.1	45.6±16.0	54.2±22.7	**84.5±23.4**
Medium Expert	51.4±25.6	71.5±28.2	60.6±22.9	**89.4±16.5**
Expert	57.7±20.5	84.8±21.0	97.3±19.1	**99.5±17.1**
Cooperative Navigation	MA-CQL	OMAR	MA-SfBC	DOM2
Random	206.0±17.5	211.3±20.3	179.8±15.7	**337.8±26.0**
Random Medium	226.5±22.1	272.6±39.4	178.8±17.9	**359.7±28.5**
Medium Replay	229.7±55.9	260.7±37.7	196.1±11.1	**324.1±38.6**
Medium	275.4±29.5	348.7±51.7	276.3±8.8	**358.9±25.2**
Medium Expert	333.3±50.1	450.3±39.0	299.8±16.8	**532.9±54.7**
Expert	478.9±29.1	564.6±8.6	553.0±41.1	**628.6±17.2**

Generalization. In MPE, we design the shifted environment by changing the speed of agents. Specifically, we change the speed of agents by randomly choosing in the region $v_j \in [v_{\min}, 1.0]$ in each episode for evaluation (the default speed of any agent j is all $v_j = 1.0$ in the standard environment). Here $v_{\min} = 0.4, 0.5, 0.3$ in the predator-prey, world, and cooperative navigation, respectively. The values are set to be the minimum speed to guarantee that the agents can all catch the adversary using the slowest speed with an appropriate policy. We train the policy using the dataset generated in the standard environment and evaluate it in the shifted environments to examine the generalization of the policy. The results are shown in the table 2. We can see that DOM2 significantly outperforms the compared algorithms in nearly all settings, and achieves the best performance in 17 out of 18 settings. Only in one setting, the performance is slightly below OMAR.

Data Efficiency. In addition to the above performance and generalization, DOM2 also possesses superior data efficiency. To demonstrate this, we train the algorithms using only a small percentage of the samples (fewer full trajectories) in the given dataset (a full dataset contains 10^6 samples). The results are shown in Figure 5 (a)-(c). The averaged normalized score is calculated by averaging the normalized score in 5 different datasets except the medium-replay (the benchmark of the normalized scores is shown in Appendix C.1). DOM2 exhibits a remarkably better performance in all MPE tasks, i.e., using a data volume that is $20\times$ times smaller, it still achieves state-of-the-art performance. Moreover, we compare our algorithm with other diffusion-based algorithms, including MA-SfBC (Chen et al., 2022) and MA-DIFF (Zhu et al., 2023) in Figure 5 (d) as the average normalized score among the MPE tasks. DOM2 also significantly outperforms existing algorithms in

Table 2: Performance comparison in **shifted environments**.

Predator Prey	MA-CQL	OMAR	MA-SfBC	DOM2
Random	1.8±5.7	10.4±3.6	9.3±15.4	**120.7±100.2**
Random Medium	4.0±7.4	41.4±20.9	22.2±34.8	**66.2±88.8**
Medium Replay	35.6±24.1	60.0±24.9	11.9±18.1	**104.2±132.5**
Medium	80.3±51.0	81.1±51.4	83.5±97.2	**95.7±79.9**
Medium Expert	69.5±44.7	78.6±59.2	84.0±86.6	**127.9±121.8**
Expert	100.0±37.1	151.7±41.3	171.6±133.6	**208.7±160.9**
World	MA-CQL	OMAR	MA-SfBC	DOM2
Random	-2.7±3.2	1.1±3.4	-1.9±4.6	**35.6±23.1**
Random Medium	-6.0±7.7	28.7±7.4	0.0±5.0	**30.3±34.2**
Medium Replay	8.1±6.2	20.1±14.5	4.6±9.2	**51.5±21.3**
Medium	33.3±11.6	32.0±15.1	35.6±15.4	**57.5±28.2**
Medium Expert	40.9±15.3	44.6±18.5	39.3±25.7	**79.9±39.7**
Expert	51.1±11.0	71.1±15.2	82.0±33.3	**91.8±34.9**
Cooperative Navigation	MA-CQL	OMAR	MA-SfBC	DOM2
Random	235.6±19.5	251.0±36.8	175.5±38.1	**265.6±57.3**
Random Medium	251.0±36.8	266.1±23.6	174.3±50.0	**304.5±45.6**
Medium Replay	224.2±30.2	271.3±33.6	191.9±54.6	**302.1±78.2**
Medium	256.5±15.2	**295.6±46.0**	285.6±68.2	295.2±80.0
Medium Expert	279.9±21.8	373.9±31.8	277.9±57.8	**439.6±89.8**
Expert	376.1±25.2	410.6±35.6	410.6±83.0	**444.0±99.0**

low-quality dataset, i.e., $10\times$ performance improvement, indicating that DOM2 is highly effective in learning from offline datasets. This unique feature is extremely useful in making good utilization of offline data, especially in applications where data collection can be costly, e.g., robotics and autonomous driving (Chi et al., 2023; Urain et al., 2023).

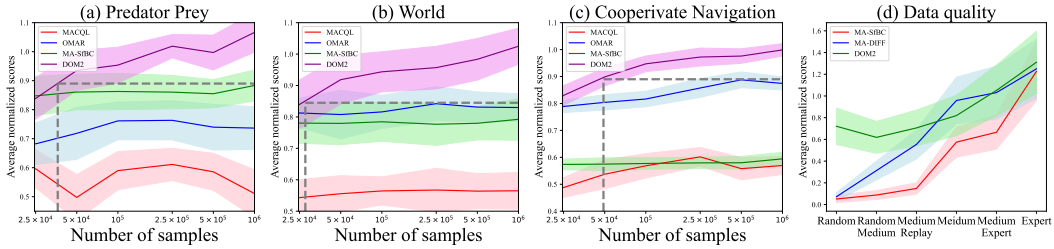

Figure 5: Algorithm performance on data-efficiency. (a)-(c) show the algorithm performance under different numbers of samples. One can see that DOM2 only requires 5% data to achieve the same performance as other baselines. (d) shows the algorithm performance under different data qualities.

5.3 Scalability in Multi-Agent MuJoCo Environment

We now turn to a more complex continuous control task: HalfCheetah-v2 environment in a multi-agent setting (extension of the single-agent task (Peng et al., 2021)). Details are in Appendix C.1.

Table 3: Performance comparison of DOM2 with MA-CQL, OMAR, and MA-SfBC.

HalfCheetah-v2	MA-CQL	OMAR	MA-SfBC	DOM2
Random	-0.1±0.2	-0.9±0.1	-388.9±29.2	**799.8±143.9**
Random Medium	-0.1±0.1	219.5±369.1	-383.1±18.4	**875.0±155.5**
Medium Replay	1216.6±514.6	1674.8±201.5	-128.3±71.3	**2564.3±216.9**
Medium	963.4±316.6	2797.0±445.7	1386.8±248.8	**2851.2±145.5**
Medium Expert	1989.8±685.6	2900.2±403.2	1392.3±190.3	**2919.6±252.8**
Expert	2722.8±1022.6	2963.8±410.5	2386.6±440.3	**3676.6±248.1**

Performance. Table 3 shows the performance of DOM2 in the multi-agent HalfCheetah-v2 environments. We see that DOM2 outperforms other compared algorithms and achieves state-of-the-art performances in all the algorithms and datasets.

Table 4: Performance comparison in **shifted environments**. We use the abbreviation "R" for Random environments and "E" for Extreme environments.

HalfCheetah-v2-R	MA-CQL	OMAR	MA-SfBC	DOM2
Random	-0.1±0.3	-1.0±0.3	-315.8±25.7	**581.8±621.0**
Random Medium	-0.2±0.3	90.8±176.2	-327.0±21.0	**1245.8±315.9**
Medium Replay	1279.6±305.4	1648.0±132.6	-171.4±43.7	**2290.8±128.5**
Medium	1111.7±585.9	2650.0±201.5	1367.6±203.9	**2788.5±112.9**
Medium Expert	1291.5±408.3	2616.6±368.8	1442.1±218.9	**2731.7±268.1**
Expert	2678.2±900.9	2295.0±357.2	2397.4±670.3	**3178.7±370.5**
HalfCheetah-v2-E	MA-CQL	OMAR	MA-SfBC	DOM2
Random	-0.1±0.1	-1.0±0.3	-309.8±23.0	**372.9±449.7**
Random Medium	-0.1±0.2	129.8±374.6	-329.2±43.6	**482.0±468.6**
Medium Replay	1290.4±230.8	1549.9±311.4	-169.8±50.5	**1904.2±201.8**
Medium	1108.1±944.0	2197.4±95.2	1355.0±195.7	**2232.4±215.1**
Medium Expert	1127.1±565.2	2196.9±186.9	1393.7±347.7	**2219.0±170.7**
Expert	2117.0±524.0	1615.7±707.6	**2757.2±200.6**	2641.3±382.9

Generalization. As in the MPE case, we also evaluate the generalization capability of DOM2 in this setting. Specifically, we design shifted environments following the scheme in Packer et al. (2018), i.e., we set up Random (R) and Extreme (E) environments by changing the environment parameters (details are shown in Appendix C.1). The performance of the algorithms is shown in Table 4. The results show that DOM2 significantly outperforms other algorithms in nearly all settings, and achieves the best performance in 11 out of 12 settings.

5.4 Ablation Study

We conduct an ablation study for DOM2, to evaluate the importance of each component in DOM2 algorithm (diffusion, regularization and data augmentation). Specifically, we compare DOM2 to four modified DOM2 algorithms, each with one different component removed or replaced. The results are shown in Figure 6. We see that removing or replacing any component in DOM2 hurts the performance across all the environments. We also investigate the sensitivity to key hyperparameters in Appendix C.5 due to the space limitation.

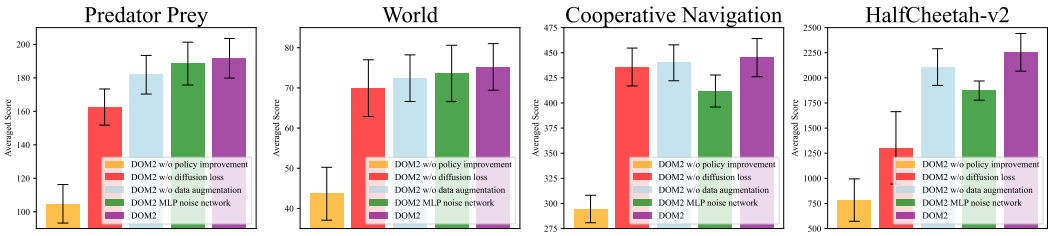

Figure 6: Impact of different algorithm components. We compare DOM2 (purple) with DOM2 w/o policy improvement (orange), DOM2 w/o diffusion loss (red), DOM2 w/o data augmentation (light-blue) and DOM2 using a MLP-based (Multi-Layer Perceptron) noise network in diffusion (green). The results show that every component of DOM2 contributes to its performance improvement.

6 Conclusion

We propose DOM2, a novel offline MARL algorithm, which contains three key components, i.e., a diffusion mechanism for enhancing policy expressiveness and diversity, an appropriate regularizer, and a data-augmentation method. Through extensive experiments on multi-agent particle and multi-agent MuJoCo environments, we show that DOM2 significantly outperforms state-of-the-art benchmarks. Moreover, DOM2 possesses superior generalization capability and ultra-high data efficiency, i.e., achieving the same performance as benchmarks with 20+ times less data.

REFERENCES

Johannes Ackermann, Volker Gabler, Takayuki Osa, and Masashi Sugiyama. Reducing overestimation bias in multi-agent domains using double centralized critics. *arXiv preprint arXiv:1910.01465*, 2019.

Anurag Ajay, Yilun Du, Abhi Gupta, Joshua Tenenbaum, Tommi Jaakkola, and Pulkit Agrawal. Is conditional generative modeling all you need for decision-making? *arXiv preprint arXiv:2211.15657*, 2022.

Fan Bao, Chongxuan Li, Jun Zhu, and Bo Zhang. Analytic-dpm: an analytic estimate of the optimal reverse variance in diffusion probabilistic models. *arXiv preprint arXiv:2201.06503*, 2022.

Huayu Chen, Cheng Lu, Chengyang Ying, Hang Su, and Jun Zhu. Offline reinforcement learning via high-fidelity generative behavior modeling. *arXiv preprint arXiv:2209.14548*, 2022.

Minshuo Chen, Kaixuan Huang, Tuo Zhao, and Mengdi Wang. Score approximation, estimation and distribution recovery of diffusion models on low-dimensional data. *arXiv preprint arXiv:2302.07194*, 2023.

Cheng Chi, Siyuan Feng, Yilun Du, Zhenjia Xu, Eric Cousineau, Benjamin Burchfiel, and Shuran Song. Diffusion policy: Visuomotor policy learning via action diffusion. *arXiv preprint arXiv:2303.04137*, 2023.

Florinel-Alin Croitoru, Vlad Hondru, Radu Tudor Ionescu, and Mubarak Shah. Diffusion models in vision: A survey. *IEEE Transactions on Pattern Analysis and Machine Intelligence*, 2023.

Christian Schroeder de Witt, Tarun Gupta, Denys Makoviichuk, Viktor Makoviychuk, Philip HS Torr, Mingfei Sun, and Shimon Whiteson. Is independent learning all you need in the starcraft multi-agent challenge? *arXiv preprint arXiv:2011.09533*, 2020.

Justin Fu, Aviral Kumar, Ofir Nachum, George Tucker, and Sergey Levine. D4rl: Datasets for deep data-driven reinforcement learning. *arXiv preprint arXiv:2004.07219*, 2020.

Scott Fujimoto and Shixiang Shane Gu. A minimalist approach to offline reinforcement learning. *Advances in neural information processing systems*, 34:20132–20145, 2021.

Scott Fujimoto, David Meger, and Doina Precup. Off-policy deep reinforcement learning without exploration. In *International conference on machine learning*, pp. 2052–2062. PMLR, 2019.

Philippe Hansen-Estruch, Ilya Kostrikov, Michael Janner, Jakub Grudzien Kuba, and Sergey Levine. Idql: Implicit q-learning as an actor-critic method with diffusion policies. *arXiv preprint arXiv:2304.10573*, 2023.

Hado Hasselt. Double q-learning. *Advances in neural information processing systems*, 23, 2010.

Jonathan Ho, Ajay Jain, and Pieter Abbeel. Denoising diffusion probabilistic models. *Advances in Neural Information Processing Systems*, 33:6840–6851, 2020.

Michael Janner, Yilun Du, Joshua B Tenenbaum, and Sergey Levine. Planning with diffusion for flexible behavior synthesis. *arXiv preprint arXiv:2205.09991*, 2022.

Jiechuan Jiang and Zongqing Lu. Offline decentralized multi-agent reinforcement learning. *arXiv preprint arXiv:2108.01832*, 2021.

Diederik Kingma, Tim Salimans, Ben Poole, and Jonathan Ho. Variational diffusion models. *Advances in neural information processing systems*, 34:21696–21707, 2021.

Diederik P Kingma and Max Welling. Auto-encoding variational bayes. *arXiv preprint arXiv:1312.6114*, 2013.

Ilya Kostrikov, Rob Fergus, Jonathan Tompson, and Ofir Nachum. Offline reinforcement learning with fisher divergence critic regularization. In *International Conference on Machine Learning*, pp. 5774–5783. PMLR, 2021a.

Ilya Kostrikov, Ashvin Nair, and Sergey Levine. Offline reinforcement learning with implicit q-learning. *arXiv preprint arXiv:2110.06169*, 2021b.

Aviral Kumar, Justin Fu, Matthew Soh, George Tucker, and Sergey Levine. Stabilizing off-policy q-learning via bootstrapping error reduction. *Advances in Neural Information Processing Systems*, 32, 2019.

Aviral Kumar, Aurick Zhou, George Tucker, and Sergey Levine. Conservative q-learning for offline reinforcement learning. *Advances in Neural Information Processing Systems*, 33:1179–1191, 2020a.

Saurabh Kumar, Aviral Kumar, Sergey Levine, and Chelsea Finn. One solution is not all you need: Few-shot extrapolation via structured maxent rl. *Advances in Neural Information Processing Systems*, 33:8198–8210, 2020b.

Sascha Lange, Thomas Gabel, and Martin Riedmiller. Batch reinforcement learning. In *Reinforcement learning*, pp. 45–73. Springer, 2012.

Seunghyun Lee, Younggyo Seo, Kimin Lee, Pieter Abbeel, and Jinwoo Shin. Offline-to-online reinforcement learning via balanced replay and pessimistic q-ensemble. In *Conference on Robot Learning*, pp. 1702–1712. PMLR, 2022.

Sergey Levine, Aviral Kumar, George Tucker, and Justin Fu. Offline reinforcement learning: Tutorial, review, and perspectives on open problems. *arXiv preprint arXiv:2005.01643*, 2020.

Timothy P Lillicrap, Jonathan J Hunt, Alexander Pritzel, Nicolas Heess, Tom Erez, Yuval Tassa, David Silver, and Daan Wierstra. Continuous control with deep reinforcement learning. *arXiv preprint arXiv:1509.02971*, 2015.

Yao Liu, Adith Swaminathan, Alekh Agarwal, and Emma Brunskill. Off-policy policy gradient with state distribution correction. *arXiv preprint arXiv:1904.08473*, 2019.

Ryan Lowe, Yi I Wu, Aviv Tamar, Jean Harb, OpenAI Pieter Abbeel, and Igor Mordatch. Multi-agent actor-critic for mixed cooperative-competitive environments. *Advances in neural information processing systems*, 30, 2017.

Cheng Lu, Yuhao Zhou, Fan Bao, Jianfei Chen, Chongxuan Li, and Jun Zhu. Dpm-solver: A fast ode solver for diffusion probabilistic model sampling in around 10 steps. *arXiv preprint arXiv:2206.00927*, 2022.

Cheng Lu, Huayu Chen, Jianfei Chen, Hang Su, Chongxuan Li, and Jun Zhu. Contrastive energy prediction for exact energy-guided diffusion sampling in offline reinforcement learning. *arXiv preprint arXiv:2304.12824*, 2023a.

Cong Lu, Philip J Ball, and Jack Parker-Holder. Synthetic experience replay. *arXiv preprint arXiv:2303.06614*, 2023b.

Laëtitia Matignon, Laurent Jeanpierre, and Abdel-Illah Mouaddib. Coordinated multi-robot exploration under communication constraints using decentralized markov decision processes. In *Twenty-sixth AAAI conference on artificial intelligence*, 2012.

Ofir Nachum, Bo Dai, Ilya Kostrikov, Yinlam Chow, Lihong Li, and Dale Schuurmans. Algaedice: Policy gradient from arbitrary experience. *arXiv preprint arXiv:1912.02074*, 2019.

Ashvin Nair, Abhishek Gupta, Murtaza Dalal, and Sergey Levine. Awac: Accelerating online reinforcement learning with offline datasets. *arXiv preprint arXiv:2006.09359*, 2020.

Alex Nichol, Prafulla Dhariwal, Aditya Ramesh, Pranav Shyam, Pamela Mishkin, Bob McGrew, Ilya Sutskever, and Mark Chen. Glide: Towards photorealistic image generation and editing with text-guided diffusion models. *arXiv preprint arXiv:2112.10741*, 2021.

Frans A Oliehoek and Christopher Amato. *A concise introduction to decentralized POMDPs*. Springer, 2016.

Frans A Oliehoek, Matthijs TJ Spaan, and Nikos Vlassis. Optimal and approximate q-value functions for decentralized pomdps. *Journal of Artificial Intelligence Research*, 32:289–353, 2008.

Charles Packer, Katelyn Gao, Jernej Kos, Philipp Krähenbühl, Vladlen Koltun, and Dawn Song. Assessing generalization in deep reinforcement learning. *arXiv preprint arXiv:1810.12282*, 2018.

Ling Pan, Longbo Huang, Tengyu Ma, and Huazhe Xu. Plan better amid conservatism: Offline multi-agent reinforcement learning with actor rectification. In *International Conference on Machine Learning*, pp. 17221–17237. PMLR, 2022.

Bei Peng, Tabish Rashid, Christian Schroeder de Witt, Pierre-Alexandre Kamienny, Philip Torr, Wendelin Böhmer, and Shimon Whiteson. Facmac: Factored multi-agent centralised policy gradients. *Advances in Neural Information Processing Systems*, 34:12208–12221, 2021.

Xue Bin Peng, Aviral Kumar, Grace Zhang, and Sergey Levine. Advantage-weighted regression: Simple and scalable off-policy reinforcement learning. *arXiv preprint arXiv:1910.00177*, 2019.

Aditya Ramesh, Prafulla Dhariwal, Alex Nichol, Casey Chu, and Mark Chen. Hierarchical text-conditional image generation with clip latents. *arXiv preprint arXiv:2204.06125*, 2022.

Tabish Rashid, Mikayel Samvelyan, Christian Schroeder, Gregory Farquhar, Jakob Foerster, and Shimon Whiteson. Qmix: Monotonic value function factorisation for deep multi-agent reinforcement learning. In *International conference on machine learning*, pp. 4295–4304. PMLR, 2018.

Shideh Rezaeifar, Robert Dadashi, Nino Vieillard, Léonard Hussenot, Olivier Bachem, Olivier Pietquin, and Matthieu Geist. Offline reinforcement learning as anti-exploration. In *Proceedings of the AAAI Conference on Artificial Intelligence*, volume 36, pp. 8106–8114, 2022.

Chitwan Saharia, William Chan, Saurabh Saxena, Lala Li, Jay Whang, Emily L Denton, Kamyar Ghasemipour, Raphael Gontijo Lopes, Burcu Karagol Ayan, Tim Salimans, et al. Photorealistic text-to-image diffusion models with deep language understanding. *Advances in Neural Information Processing Systems*, 35:36479–36494, 2022.

Noah Y Siegel, Jost Tobias Springenberg, Felix Berkenkamp, Abbas Abdolmaleki, Michael Neunert, Thomas Lampe, Roland Hafner, Nicolas Heess, and Martin Riedmiller. Keep doing what worked: Behavioral modelling priors for offline reinforcement learning. *arXiv preprint arXiv:2002.08396*, 2020.

Jascha Sohl-Dickstein, Eric Weiss, Niru Maheswaranathan, and Surya Ganguli. Deep unsupervised learning using nonequilibrium thermodynamics. In *International Conference on Machine Learning*, pp. 2256–2265. PMLR, 2015.

Jiaming Song, Chenlin Meng, and Stefano Ermon. Denoising diffusion implicit models. *arXiv preprint arXiv:2010.02502*, 2020a.

Yang Song and Stefano Ermon. Generative modeling by estimating gradients of the data distribution. *Advances in Neural Information Processing Systems*, 32, 2019.

Yang Song, Jascha Sohl-Dickstein, Diederik P Kingma, Abhishek Kumar, Stefano Ermon, and Ben Poole. Score-based generative modeling through stochastic differential equations. *arXiv preprint arXiv:2011.13456*, 2020b.

Peter Sunehag, Guy Lever, Audrunas Gruslys, Wojciech Marian Czarnecki, Vinicius Zambaldi, Max Jaderberg, Marc Lanctot, Nicolas Sonnerat, Joel Z Leibo, Karl Tuyls, et al. Value-decomposition networks for cooperative multi-agent learning. *arXiv preprint arXiv:1706.05296*, 2017.

Adith Swaminathan and Thorsten Joachims. Batch learning from logged bandit feedback through counterfactual risk minimization. *The Journal of Machine Learning Research*, 16(1):1731–1755, 2015.

Ardi Tampuu, Tambet Matiisen, Dorian Kodelja, Ilya Kuzovkin, Kristjan Korjus, Juhan Aru, Jaan Aru, and Raul Vicente. Multiagent cooperation and competition with deep reinforcement learning. *PloS one*, 12(4):e0172395, 2017.

Brandon Trabucco, Kyle Doherty, Max Gurinas, and Ruslan Salakhutdinov. Effective data augmentation with diffusion models. *arXiv preprint arXiv:2302.07944*, 2023.

Julen Urain, Niklas Funk, Jan Peters, and Georgia Chalvatzaki. Se (3)-diffusionfields: Learning smooth cost functions for joint grasp and motion optimization through diffusion. In *2023 IEEE International Conference on Robotics and Automation (ICRA)*, pp. 5923–5930. IEEE, 2023.

Zhendong Wang, Jonathan J Hunt, and Mingyuan Zhou. Diffusion policies as an expressive policy class for offline reinforcement learning. *arXiv preprint arXiv:2208.06193*, 2022.

Yifan Wu, George Tucker, and Ofir Nachum. Behavior regularized offline reinforcement learning. *arXiv preprint arXiv:1911.11361*, 2019.

Zhisheng Xiao, Karsten Kreis, and Arash Vahdat. Tackling the generative learning trilemma with denoising diffusion gans. *arXiv preprint arXiv:2112.07804*, 2021.

Yiqin Yang, Xiaoteng Ma, Chenghao Li, Zewu Zheng, Qiyuan Zhang, Gao Huang, Jun Yang, and Qianchuan Zhao. Believe what you see: Implicit constraint approach for offline multi-agent reinforcement learning. *Advances in Neural Information Processing Systems*, 34:10299–10312, 2021.

Chao Yu, Akash Velu, Eugene Vinitsky, Yu Wang, Alexandre Bayen, and Yi Wu. The surprising effectiveness of ppo in cooperative, multi-agent games. *arXiv preprint arXiv:2103.01955*, 2021.

Zhengbang Zhu, Minghuan Liu, Liyuan Mao, Bingyi Kang, Minkai Xu, Yong Yu, Stefano Ermon, and Weinan Zhang. Madiff: Offline multi-agent learning with diffusion models. *arXiv preprint arXiv:2305.17330*, 2023.

Appendix

A Related Work

Due to the page limitation, we propose the related work in the supplementary materials as below consisting of the offline reinforcement learning (Offline RL), multi-agent reinforcement learning (MARL) and the diffusion models.

Offline RL and MARL: Distribution shift is a key obstacle in offline RL and multiple methods have been proposed to tackle the problem based on conservatism to constrain the policy or Q-value by regularizers (Wu et al., 2019; Kumar et al., 2019; Fujimoto et al., 2019; Kumar et al., 2020a). Policy regularization ensures the policy to be close to the behavior policy via a policy regularizer, e.g., BRAC (Wu et al., 2019), BEAR (Kumar et al., 2019), BCQ (Fujimoto et al., 2019), TD3+BC (Fujimoto & Gu, 2021), implicit update (Peng et al., 2019; Siegel et al., 2020; Nair et al., 2020) and importance sampling (Kostrikov et al., 2021a; Swaminathan & Joachims, 2015; Liu et al., 2019; Nachum et al., 2019)). Critic regularization instead constrains the Q-values for stability, e.g., CQL (Kumar et al., 2020a), IQL (Implicit Q-Learning) (Kostrikov et al., 2021b), and TD3-CVAE (Rezaeifar et al., 2022). On the other hand, Multi-Agent Reinforcement Learning (MARL) has made significant process, such as MADDPG (Lowe et al., 2017), MAPPO (Yu et al., 2021), VDN (Sunehag et al., 2017) and QMIX (Rashid et al., 2018) under the centralized training with decentralized execution (CTDE) paradigm (Oliehoek et al., 2008; Matignon et al., 2012), and IQL (Independent Q-Learning) (Tampuu et al., 2017), MATD3 (Ackermann et al., 2019) and IPPO (de Witt et al., 2020) are designed as fully decentralized training and execution scheme. The offline MARL problem has also attracted attention using conservatism-based methods, e.g., MA-BCQ (Jiang & Lu, 2021), MA-ICQ (Yang et al., 2021), MA-CQL and OMAR (Pan et al., 2022).

Diffusion Models: Diffusion model (Ho et al., 2020; Song et al., 2020b; Sohl-Dickstein et al., 2015; Song & Ermon, 2019; Song et al., 2020a), a specific type of generative model, has shown significant success in various applications, especially in generating images from text descriptions (Nichol et al., 2021; Ramesh et al., 2022; Saharia et al., 2022)). Recent works have focused on the foundation of diffusion models, e.g., the statistical theory (Chen et al., 2023), and the accelerating method for sampling (Lu et al., 2022; Bao et al., 2022). Generative model has been applied to policy modeling, including conditional VAE (Kingma & Welling, 2013), diffusers (Janner et al., 2022; Ajay et al., 2022), Diffusion-QL (Wang et al., 2022), SfBC (Chen et al., 2022; Lu et al., 2023a) and IDQL (Hansen-Estruch et al., 2023) in the single-agent setting and MA-DIFF (Zhu et al., 2023) in multi-agent setting. Our method successfully introduces the diffusion model with the accelerated solver to offline multi-agent settings under the fully decentralized training and execution procedure beyond conservatism.

B Additional Details about Diffusion Probabilistic Model

In this section, we elaborate on more details about the diffusion probabilistic model that we do not cover in Section 4.1 due to space limitation, and compare the similar parts between the diffusion model and DOM2 in offline MARL.

In the noising action part, we emphasize a forward process $\{\boldsymbol{b}_{t,j}^{\tau}\}_{\tau\in[\tau_0,\tau_N]}$ starting at $\boldsymbol{b}_{t,j}^{\tau_0} \sim \boldsymbol{\pi}_{\boldsymbol{\theta}_j}(\cdot|\boldsymbol{o}_{t,j})$ in the dataset $\mathcal{D}$ and $\boldsymbol{b}_{t,j}^{\tau_N}$ is the final noise. This forward process satisfies that for any diffusing time index $\tau \in [\tau_0, \tau_N]$, the transition probability $q_{\tau_0\tau}(\boldsymbol{b}_{t,j}^{\tau}|\boldsymbol{b}_{t,j}^{\tau_0}) = \mathcal{N}(\boldsymbol{b}_{t,j}^{\tau}; \alpha_\tau \boldsymbol{b}_{t,j}^{\tau_0}, \sigma_\tau^2 \boldsymbol{I})$ (Lu et al., 2022) (α_τ, σ_τ is called the noise schedule). We build the reverse process of SDE as Equation 2 and we will describe the connection between the forward process and the reverse process of SDE. Kingma (Kingma et al., 2021) proves that the following forward SDE (Equation 6) solves to a process whose transition probability $q_{\tau_0\tau}(\boldsymbol{b}_{t,j}^{\tau}|\boldsymbol{b}_{t,j}^{\tau_0})$ is the same as the forward process, which is written as:

$$\mathrm{d}\boldsymbol{b}_{t,j}^{\tau} = f(\tau)\boldsymbol{b}_{t,j}^{\tau}\mathrm{d}\tau + g(\tau)\mathrm{d}\boldsymbol{w}_\tau, \quad \boldsymbol{b}_{t,j}^{\tau_0} \sim \boldsymbol{\pi}_{\boldsymbol{\beta}_j}(\cdot|\boldsymbol{o}_{t,j}). \tag{6}$$

Here $\boldsymbol{\pi}_{\boldsymbol{\beta}_j}(\cdot|\boldsymbol{o}_{t,j})$ is the behavior policy to generate $\boldsymbol{b}_{t,j}^{\tau_0}$ for agent j given the observation $\boldsymbol{o}_{t,j}$, $f(\tau) = \frac{\mathrm{d}\log\alpha_\tau}{\mathrm{d}\tau}$, $g^2(\tau) = \frac{\mathrm{d}\sigma_\tau^2}{\mathrm{d}\tau} - 2\frac{\mathrm{d}\log\alpha_\tau}{\mathrm{d}\tau}\sigma_\tau^2$ and $\boldsymbol{w}_t$ is a standard Brownion motion. It was proven in Song et al. (2020b) that the forward process of SDE from τ_0 to τ_N has an equivalent reverse process of the SDE from τ_N to τ_0, which is the Equation 2. In this way, the forward process of conditional probability and the reverse process of SDE are connected.

In our DOM2 for offline MARL, we propose the objective function in Equation 3 and its simplification. In detail, following Lu et al. (2022), the loss function for score matching is defined as:

$$\begin{aligned}\mathcal{L}_{bc}(\boldsymbol{\theta}_j) &:= \int_{\tau_0}^{\tau_N} \omega(\tau)\mathbb{E}_{\boldsymbol{a}_{t,j}^{\tau}\sim q_\tau(\boldsymbol{b}_{t,j}^{\tau})}[\|\boldsymbol{\epsilon}_{\boldsymbol{\theta}_j}(\boldsymbol{a}_{t,j}^{\tau},\boldsymbol{o}_{t,j},\tau)+\sigma_\tau\nabla_{\boldsymbol{b}_{t,j}^{\tau}}\log q_\tau(\boldsymbol{b}_{t,j}^{\tau}|\boldsymbol{o}_{t,j})\|_2^2]\mathrm{d}\tau \\ &= \int_{\tau_0}^{\tau_N} \omega(\tau)\mathbb{E}_{\boldsymbol{a}_{t,j}^{\tau_0}\sim\boldsymbol{\pi}_{\boldsymbol{\beta}_j}(\boldsymbol{a}_{t,j}^{\tau_0}|\boldsymbol{o}_{t,j}),\epsilon\sim\mathcal{N}(\mathbf{0},\boldsymbol{I})}[\|\boldsymbol{\epsilon}-\boldsymbol{\epsilon}_{\boldsymbol{\theta}_j}(\alpha_\tau\boldsymbol{a}_{t,j}^{\tau_0}+\sigma_\tau\boldsymbol{\epsilon},\boldsymbol{o}_{t,j},\tau)\|_2^2]\mathrm{d}\tau+C,\end{aligned} \tag{7}$$

where $\omega(\tau)$ is the weighted parameter and C is a constant independent of $\boldsymbol{\theta}_j$. In practice for simplification, we set that $w(\tau)=1/(\tau_N-\tau_0)$, replace the integration by random sampling a diffusion timestep and ignore the equally weighted parameter $\omega(\tau)$ and the constant C. After these simplifications, the final objective becomes Equation 3.

Next, we introduce the accelerated sampling method to build the connection between the reverse process of SDE for sampling and the accelerated DPM-solver.

In the denoising part, we utilize the following SDE of the reverse process (Equation (2.5) in Lu et al. (2022)) as:

$$\mathrm{d}\boldsymbol{a}_{t,j}^{\tau}=\left[f(\tau)\boldsymbol{a}_{t,j}^{\tau}+\frac{g^2(\tau)}{\sigma_\tau}\boldsymbol{\epsilon}_{\boldsymbol{\theta}_j}(\boldsymbol{a}_{t,j}^{\tau},\boldsymbol{o}_{t,j},\tau)\right]\mathrm{d}\tau+g(\tau)\mathrm{d}\overline{\boldsymbol{w}}_\tau,\quad \boldsymbol{a}_{t,j}^{\tau_N}\sim\mathcal{N}(\mathbf{0},\boldsymbol{I}). \tag{8}$$

To achieve faster sampling, Song et al. (2020b) proves that the following ODE equivalently describes the process given by the reverse diffusion SDE. It is thus called the diffusion ODE.

$$\frac{\mathrm{d}\boldsymbol{a}_{t,j}^{\tau}}{\mathrm{d}\tau}=f(\tau)\boldsymbol{a}_{t,j}^{\tau}+\frac{g^2(\tau)}{2\sigma_\tau}\boldsymbol{\epsilon}_{\boldsymbol{\theta}_j}(\boldsymbol{a}_{t,j}^{\tau},\boldsymbol{o}_{t,j},\tau),\quad \boldsymbol{a}_{t,j}^{\tau_N}\sim\mathcal{N}(\mathbf{0},\boldsymbol{I}). \tag{9}$$

At the end of the denoising part, we use the efficient DPM-solver (Equation 4) to solve the diffusion ODE and thus implement the denoising process. The formal derivation can be found on Lu et al. (2022) and we restate their argument here for the sake of completeness, for a more detailed explanation, please refer to Lu et al. (2022).

For such a semi-linear structured ODE in Equation 9, the solution at time τ can be formulated as:

$$\boldsymbol{a}_{t,j}^{\tau}=\exp\left(\int_{\tau'}^{\tau}f(u)\mathrm{d}u\right)\boldsymbol{a}_{t,j}^{\tau'}+\int_{\tau'}^{\tau}\left(\exp\left(\int_{u}^{\tau}f(z)\mathrm{d}z\right)\frac{g^2(u)}{2\sigma_u}\boldsymbol{\epsilon}_{\boldsymbol{\theta}_j}(\boldsymbol{a}_{t,j}^{u},\boldsymbol{o}_{t,j},u)\right)\mathrm{d}u. \tag{10}$$

Defining $\lambda_\tau=\log(\alpha_\tau/\sigma_\tau)$, we can rewrite the solution as:

$$\boldsymbol{a}_{t,j}^{\tau}=\frac{\alpha_\tau}{\alpha_\tau'}\boldsymbol{a}_{t,j}^{\tau'}-\alpha_\tau\int_{\tau'}^{\tau}\left(\frac{\mathrm{d}\lambda_u}{\mathrm{d}u}\right)\frac{\sigma_u}{\alpha_u}\boldsymbol{\epsilon}_{\boldsymbol{\theta}_j}(\boldsymbol{a}_{t,j}^{u},\boldsymbol{o}_{t,j},u)\mathrm{d}u. \tag{11}$$

Notice that the definition of λ_τ is dependent on the noise schedule α_τ,σ_τ. If λ_τ is a continuous and strictly decreasing function of τ (the selection of our final noise schedule in Equation 13 actually satisfies this requirement, which we will discuss afterwards), we can rewrite the term by *change-of-variable*. Based on the inverse function $\tau_\lambda(\cdot)$ from λ to τ such that $\tau=\tau_\lambda(\lambda_\tau)$ (for simplicity we can also write this term as τ_λ) and define $\hat{\boldsymbol{\epsilon}}_{\boldsymbol{\theta}_j}(\hat{\boldsymbol{a}}_{t,j}^{\lambda_\tau},\boldsymbol{o}_{t,j},\lambda_\tau)=\boldsymbol{\epsilon}_{\boldsymbol{\theta}_j}(\boldsymbol{a}_{t,j}^{\tau},\boldsymbol{o}_{t,j},\tau)$, we can rewrite Equation 11 as:

$$\boldsymbol{a}_{t,j}^{\tau}=\frac{\alpha_\tau}{\alpha_\tau'}\boldsymbol{a}_{t,j}^{\tau'}-\alpha_\tau\int_{\lambda_{\tau'}}^{\lambda_\tau}\exp(-\lambda)\hat{\boldsymbol{\epsilon}}_{\boldsymbol{\theta}_j}(\hat{\boldsymbol{a}}_{t,j}^{\lambda},\boldsymbol{o}_{t,j},\lambda)\mathrm{d}\lambda. \tag{12}$$

Equation 12 is satisfied for any $\tau,\tau'\in[\tau_0,\tau_N]$. We uniformly partition the diffusion horizon $[\tau_0,\tau_N]$ into N subintervals $\{[\tau_i,\tau_{i+1}]\}_{i=0}^{N-1}$, where $\tau_i=i/N$ (also $\tau_0=0,\tau_N=1$). We follow Xiao et al. (2021) to use the variance-preserving (VP) type function (Ho et al., 2020; Song et al., 2020b; Lu et al., 2022) to train the policy efficiently. First, define $\{\beta_\tau\}_{\tau\in[0,1]}$ by

$$\beta_\tau=1-\exp\left(-\beta_{\min}\frac{1}{(N+1)}-(\beta_{\max}-\beta_{\min})\frac{2N\tau+1}{2(N+1)^2}\right), \tag{13}$$

and we pick $\beta_{\min}=0.1,\beta_{\max}=20.0$. Then we choose the noise schedule $\alpha_{\tau_i},\sigma_{\tau_i}$ by $\alpha_{\tau_i}=1-\beta_{\tau_i},\sigma_{\tau_i}^2=1-\alpha_{\tau_i}^2$ for $i=1\ldots N$. It can be then verified that by plugging this particular

choice of α_τ and σ_τ into $\lambda_\tau = \log(\alpha_\tau/\sigma_\tau)$, the obtained λ_τ is a strictly decreasing function of τ (Appendix E in Lu et al. (2022)).

In each interval $[\tau_{i-1}, \tau_i]$, given $\boldsymbol{a}_{t,j}^{\tau_i}$, the action obtained in the previous diffusion step at τ_i, according to Equation 12, the exact action in the next step denoted as $\boldsymbol{a}_{t,j}^{\tau_{i-1}}$ is given by:

$$\boldsymbol{a}_{t,j}^{\tau_{i-1}} = \frac{\alpha_{\tau_{i-1}}}{\alpha_{\tau_i}} \boldsymbol{a}_{t,j}^{\tau_i} - \alpha_{\tau_i} \int_{\lambda_{\tau_i}}^{\lambda_{\tau_{i-1}}} \exp(-\lambda) \hat{\boldsymbol{\epsilon}}_{\boldsymbol{\theta}_j}(\hat{\boldsymbol{a}}_{t,j}^{\lambda}, \boldsymbol{o}_{t,j}, \lambda) \mathrm{d}\lambda. \tag{14}$$

We take the k-th order Taylor expansion for $\hat{\boldsymbol{\epsilon}}_{\boldsymbol{\theta}_j}(\hat{\boldsymbol{a}}_{t,j}^{\lambda}, \boldsymbol{o}_{t,j}, \lambda)$ at λ_{τ_i} and denote the derivative of $\hat{\boldsymbol{\epsilon}}_{\boldsymbol{\theta}_j}(\hat{\boldsymbol{a}}_{t,j}^{\lambda}, \boldsymbol{o}_{t,j}, \lambda)$ in the k-th order as $\hat{\boldsymbol{\epsilon}}_{\boldsymbol{\theta}_j}^{(k)}(\hat{\boldsymbol{a}}_{t,j}^{\lambda}, \boldsymbol{o}_{t,j}, \lambda_{\tau_i})$. By ignoring the higher-order remainder $\mathcal{O}((\lambda_{\tau_{i-1}} - \lambda_{\tau_i})^{k+1})$, the k-th order DPM-solver for sampling can be written as:

$$\boldsymbol{a}_{t,j}^{\tau_{i-1}} = \frac{\alpha_{\tau_{i-1}}}{\alpha_{\tau_i}} \boldsymbol{a}_{t,j}^{\tau_i} - \alpha_{\tau_i} \sum_{n=0}^{k-1} \hat{\boldsymbol{\epsilon}}_{\boldsymbol{\theta}_j}^{(n)}(\hat{\boldsymbol{a}}_{t,j}^{\lambda_{\tau_i}}, \boldsymbol{o}_{t,j}, \lambda_{\tau_i}) \int_{\lambda_{\tau_i}}^{\lambda_{\tau_{i-1}}} \exp(-\lambda) \frac{(\lambda - \lambda_{\tau_i})^n}{n!} \mathrm{d}\lambda. \tag{15}$$

For $k = 1$, the results are actually the first-order iteration function in Section 4.1. Similarly, we can use a higher-order DPM-solver.

C Experimental Details

C.1 Experimental Setup: Environments

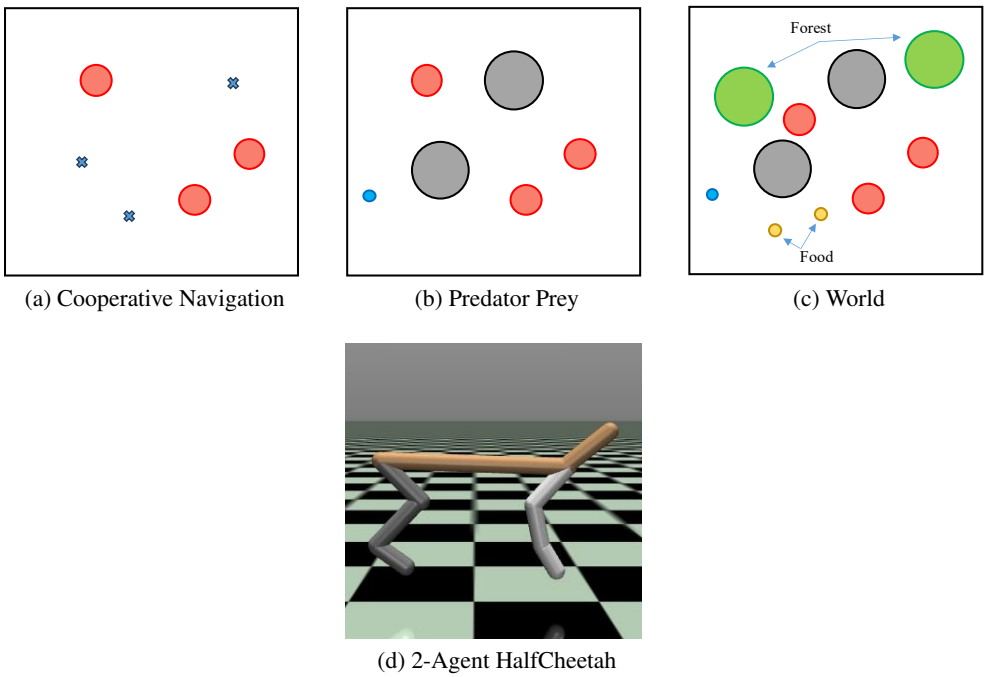

(a) Cooperative Navigation (b) Predator Prey (c) World

(d) 2-Agent HalfCheetah

Figure 7: Multi-agent particle environments (MPE) and Multi-agent HalfCheetah task in MuJoCo Environment (MAMuJoCo).

We implement our algorithm and baselines based on the open-source environmental engines of multi-agent particle environments (MPE) (Lowe et al., 2017),[1] and multi-agent MuJoCo environments (MAMuJoCo) (Peng et al., 2021)[2]. Figure 7 shows the tasks in MPE and MAMuJoCo. In

[1] https://github.com/openai/multiagent-particle-envs

[2] https://github.com/schroederdewitt/multiagent_mujoco

cooperative navigation shown in Figure 7a, agents (red dots) cooperate to reach the landmark (blue crosses) without collision. In predator-prey in Figure 7b, predators (red dots) are intended to catch the prey (blue dots) and avoid collision with the landmark (grey dots). The predators need to cooperate with each other to surround and catch the prey because the predators run slower than the prey. The world task in Figure 7c consists of 3 agents (red dots) and 1 adversary (blue dots). The slower agents are intended to catch the faster adversary that desires to eat food (yellow dots). The agents need to avoid collision with the landmark (grey dots). Moreover, if the adversary hides in the forest (green dots), it is harder for the agents to catch the adversary because they do not know the position of the adversary. The two-agent HalfCheetah is shown in Figure 7d, and different agents control different joints (grey and white joints) and they need to cooperate for better control the half-shaped cheetah to run stably and fast. The expert and random scores (a.k.a., mean episode returns) for cooperative navigation, predator-prey, and world are $\{516.8, 159.8\}, \{185.6, -4.1\}, \{79.5, -6.8\}$, and we use these scores to calculate the normalized scores in Figure 5.

For the MAMuJoCo environment, we design two different shifted environments: Random (R) environment and Extreme (E) environments following Packer et al. (2018). These environments have different parameters and we focus on randomly sampling the three parameters: (1) power, the parameter to influence the force that is multiplied before application, (2) torso density, the parameter to influence the weight, (3) sliding friction of the joints. The detailed sample regions of these parameters in different environments are shown in table 5.

Table 5: Range of parameters in the Multi-MuJoCo HalfCheetah-v2 environment.

	Deterministic	Random	Extreme
Power	1.0	[0.8,1.2]	[0.6,0.8]∪[1.2,1.4]
Density	1000	[750,1250]	[500,750]∪[1250,1500]
Friction	0.4	[0.25,0.55]	[0.1,0.25]∪[0.55,0.7]

C.2 Experimental Setup: Network Structures and Hyperparameters

In DOM2, we utilize the multi-layer perceptron (MLP) to model the Q-value functions of the critics by concatenating the state-action pairs and sending them into the MLP to generate the Q-function, which is the same as in MA-CQL and OMAR (Pan et al., 2022). Different from MA-CQL and OMAR that uses MLP for action generation, we utilize the diffusion policy to generate actions. We use a multi-layer residual network to model the noise network $\boldsymbol{\epsilon}_{\boldsymbol{\theta}_j}(\boldsymbol{a}_{t,j}^{\tau_i}, \boldsymbol{o}_{t,j}, \tau_i)$ for agent j at timestep τ_i, which ensembles the U-Net architecture (Chen et al., 2022; Janner et al., 2022). One difference is that we use a dropout layer with a 0.1 dropout rate in each residual network component for preventing overfitting and better training stability.

All the MLPs consist of 1 batch normalization layer, 2 hidden layers, and 1 output layer with the size $(\mathrm{input\_dim}, \mathrm{hidden\_dim}), (\mathrm{hidden\_dim}, \mathrm{hidden\_dim}), (\mathrm{hidden\_dim}, \mathrm{output\_dim})$ and $\mathrm{hidden\_dim} = 256$. In the hidden layers, the output is activated with the Mish function, and the output of the output layer is activated with the Tanh function.

For training the Q-value network, we use the learning rate of 3×10^{-4} in all environments. In policy training, we use 5×10^{-3} in all MPE environments as the learning rate to train the noise network (Figure 8) in the diffusion policy. In the MAMuJoCo HalfCheetah-v2 environment, the learning rates for training the noise network in random, random-medium, medium-replay, medium, medium-expert, and expert datasets are set to $1\times10^{-3}, 2.5\times10^{-4}, 1\times10^{-4}, 2.5\times10^{-4}, 2.5\times10^{-4}, 5\times10^{-4}$, respectively. The total diffusion step number N is for sampling denoised actions. We use $N = 5$ as the diffusion timestep in MPE and $N = 10$ in the MAMuJoCo HalfCheetah-v2 environment. The trade-off parameter η is used to balance the regularizers of actor losses and the threshold values $\mathcal{R} = \{r_{\text{th},1}, ..., r_{\text{th},K}\}$ are set for efficient data augmentation. The hyperparameter η and the set of threshold values $\mathcal{R} = \{r_{\text{th},1}, ..., r_{\text{th},K}\}$ in different settings are shown in table 6. For all other hyperparameters, we use the same values in our experiments.

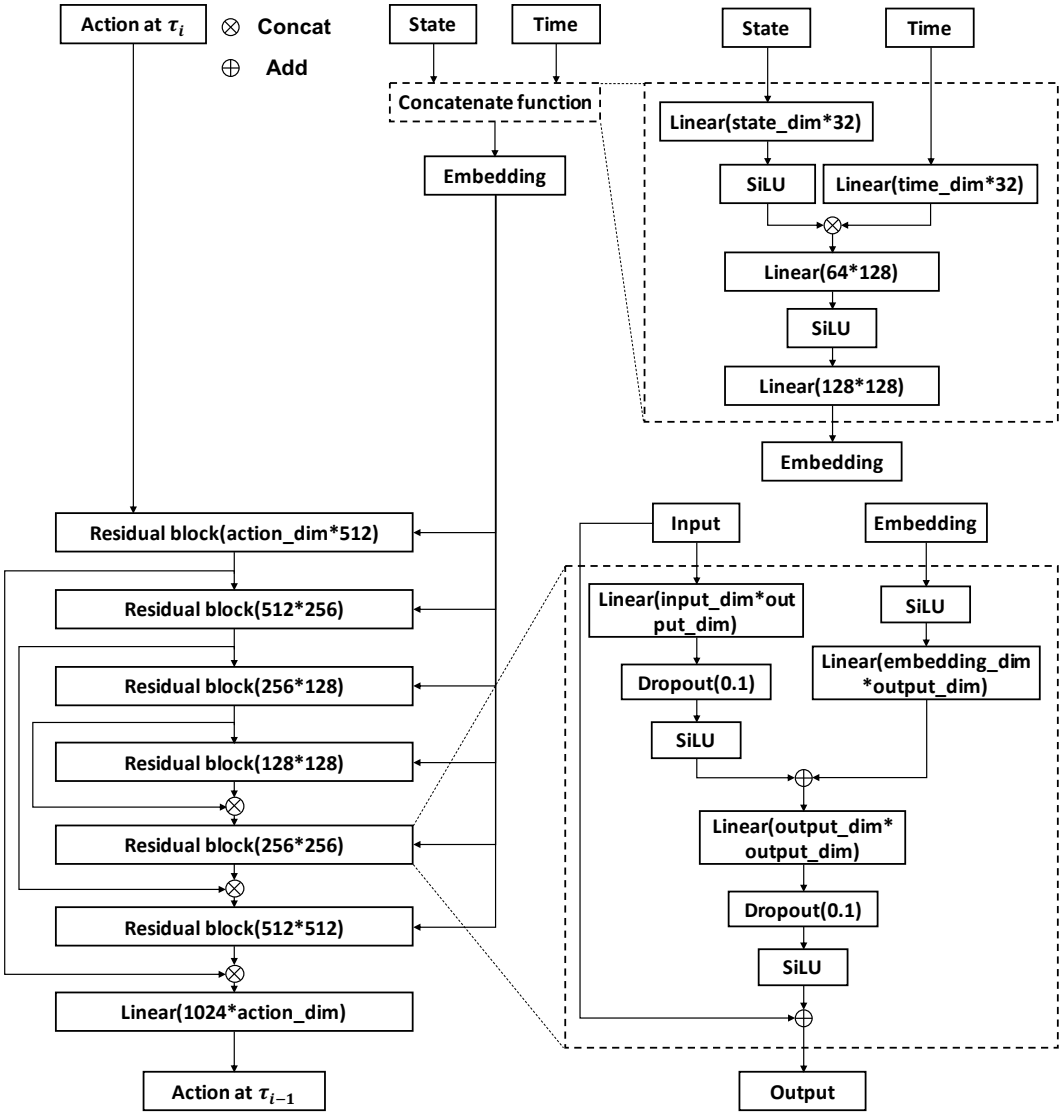

Figure 8: Architecture of the noise network ϵ_{θ_j} as is a multi-layer residual network that resembles the structure of U-Net (Ho et al., 2020; Chen et al., 2022). Different from Chen et al. (2022), we include a dropout layer for training stability.

Table 6: The η value and the set of threshold values $\mathcal{R}$ in DOM2.

Predator Prey	η	Set of threshold values $\mathcal{R}$
Random	25.0	None
Random Medium	250.0	$[100.0, 150.0, 200.0, 250.0, 300.0]$
Medium Replay	5.0	$[0.0, 10.0, 20.0, 30.0, 40.0, 50.0, 60.0, 70.0, 80.0, 90.0, 100.0]$
Medium	2.5	$[100.0, 150.0, 200.0, 250.0, 300.0]$
Medium Expert	25.0	$[100.0, 150.0, 200.0, 250.0, 300.0, 350.0, 400.0]$
Expert	0.5	$[200.0, 250.0, 300.0, 350.0, 400.0]$
World	η	Set of threshold values $\mathcal{R}$
Random	5.0	None
Random Medium	25.0	$[65.5, 86.4, 101.5, 101.5]$
Medium Replay	2.5	$[-3.7, 5.9, 15.6, 15.6]$
Medium	0.5	$[65.5, 86.4, 101.5, 101.5]$
Medium Expert	0.5	$[50.0, 75.0, 100.0, 125.0, 150.0, 175.0]$
Expert	0.5	$[75.0, 100.0, 125.0, 150.0, 175.0]$
Cooperative Navigation	η	Set of threshold values $\mathcal{R}$
Random	10000.0	None
Random Medium	500.0	$[200.0, 250.0, 300.0, 350.0, 400.0, 450.0, 500.0, 550.0]$
Medium Replay	500.0	$[0.0, 10.0, 20.0, 30.0, 40.0, 50.0, 60.0, 70.0, 80.0, 90.0, 100.0]$
Medium	250.0	$[200.0, 250.0, 300.0, 350.0, 400.0, 450.0, 500.0, 550.0]$
Medium Expert	250.0	$[264.4, 267.3, 333.5, 336.4, 385.3, 385.3, 387.9, 387.9]$
Expert	50.0	$[525.0, 550.0, 575.0, 600.0, 625.0]$
HalfCheetah-v2	η	Set of threshold values $\mathcal{R}$
Random	0.5	None
Random Medium	0.5	$[1800.0, 1850.0, 1900.0, 1950.0, 2000.0]$
Medium Replay	1.0	$[100.0, 300.0, 500.0, 1000.0, 1500.0]$
Medium	2.5	$[1800.0, 1850.0, 1900.0, 1950.0, 2000.0]$
Medium Expert	2.5	$[1631.6, 1692.5, 1735.5, 1735.5]$
Expert	0.05	$[3800.0, 3850.0, 3900.0, 3950.0, 4000.0]$

C.3 Experimental Setup: Dataset construction

We construct 6 different datasets following Fu et al. (2020) to represent different qualities of behavior policies: i) Random dataset: take 1 million samples by unrolling a randomly initialized policy, ii) Medium-replay dataset: record all of the samples in the replay buffer during training until the performance of the policy is at the medium level, iii) Medium dataset: take 1 million samples by unrolling a policy whose performance reaches the medium level, vi) Expert dataset: take 1 million samples by unrolling a well-trained policy, v) Random-medium dataset: take 1 million samples by sampling the random dataset and the medium dataset in proportion (90% random dataset and 10% medium dataset in MPE, 99.9% random dataset and 0.1% medium dataset in MAMuJoCo). and vi) Medium-expert dataset: take 1 million samples by sampling the medium dataset and the expert dataset in proportion (90% medium dataset and 10% expert dataset in MPE, 99.9% medium dataset and 0.1% expert dataset in MAMuJoCo).

C.4 Details about 3-Agent 6-Landmark Task

We now discuss detailed results in the 3-Agent 6-Landmark task. We construct the environment based on the cooperative navigation task in multi-agent particles environment (Lowe et al., 2017). This task contains 3 agents and 6 landmarks. The size of agents and landmarks are all 0.1. For any landmark $j = 0, 1, ..., 5$, its position is given by $(\cos(\frac{2\pi j}{6}), \sin(\frac{2\pi j}{6}))$. In each episode, the environment initializes the positions of 3 agents inside the circle of the center $(0, 0)$ with a 0.1 radius uniformly at random. If the agent can successfully find any one of the landmarks, the agent gains a positive reward. If two agents collide, the agents are both penalized with a negative reward.

We construct two different environments: the standard environment and shifted environment. In the standard environment, all 6 landmarks exist in the environment, while in the shifted environment, in each episode, we randomly hide 3 out of 6 landmarks. We collect data generated from the standard environment and train the agents using different algorithms for both environments.

We evaluate how our algorithm performs compared to the baseline algorithms in this task (with different configurations of the targets) and investigate their performance by rolling out K times at each evaluation ($K \in \{1, 10\}$) following Kumar et al. (2020b). For evaluating the policy in the standard environment, we test the policy for 10 episodes with different initialized positions and calculate the mean value (a.k.a, mean episode returns, same below) and the standard deviation as the results of evaluating the policy. This corresponds to rolling out $K = 1$ time at each evaluation. For the shifted environment, in spite of the former evaluation method ($K = 1$), we also evaluate the algorithm in another way following Kumar et al. (2020b). We first test the policy for 10 episodes at the same initialized positions and take the maximum return in these 10 episodes. We repeat this procedure 10 times with different initialized positions and calculate the mean value and the standard deviation as the results of evaluating the policy, which corresponds to rolling out $K = 10$ times at each evaluation. It has been reported (see Kumar et al. (2020b)) that for a diversity-driven method, increasing K can help the diverse policy gain higher returns.

In table 7, we show the results (the mean episode returns) of different algorithms in standard environments and shifted environments. It can be seen that DOM2 outperforms other algorithms in both the standard environment and shifted environments. Specifically, in the standard environment, DOM2 outperforms other algorithms. This shows that DOM2 has better expressiveness compared to other algorithms. In the shifted environment, when $K = 1$, it turns out that DOM2 already achieves better performance with expressiveness. Moreover, when $K = 10$, DOM2 significantly improves the performance compared to the results in the $K = 1$ setting. This implies that DOM2 finds much more diverse policies, thus achieving better performance compared to the existing conservatism-based method, i.e., MA-CQL and OMAR.

Table 7: Comparison of DOM2 with other algorithms in 3-Agent 6-Landmark settings.

Standard-$K = 1$	MA-CQL	OMAR	MA-SfBC	DOM2
Random	321.2±39.1	326.0±39.4	198.5±23.5	**470.0±70.0**
Random Medium	237.4±48.2	237.8±55.9	201.5±19.0	**329.9±60.0**
Medium Replay	396.9±40.1	455.7±52.5	339.3±29.5	**542.4±32.5**
Medium	267.4±37.2	349.9±20.7	459.9±25.2	**532.5±55.2**
Medium Expert	300.9±77.4	395.5±91.0	552.1±16.9	**678.7±4.4**
Expert	457.5±110.0	595.0±54.7	606.1±13.9	**683.3±2.1**
Shifted-$K = 1$	MA-CQL	OMAR	MA-SfBC	DOM2
Random	177.5±24.4	178.4±34.3	142.2±13.0	**262.5±42.7**
Random Medium	157.0±33.4	153.3±31.5	147.2±13.4	**196.2±31.8**
Medium Replay	247.0±43.4	274.4±18.0	205.7±37.5	**317.2±54.7**
Medium	171.6±21.8	214.0±18.0	276.7±48.9	**284.8±37.6**
Medium Expert	201.2±54.7	241.9±32.2	328.7±45.9	**382.3±36.4**
Expert	258.1±67.5	334.0±21.7	374.2±28.5	**393.1±43.3**
Shifted-$K = 10$	MA-CQL	OMAR	MA-SfBC	DOM2
Random	186.8±13.9	186.7±30.1	203.5±12.2	**283.7±53.0**
Random Medium	160.8±31.4	164.5±37.7	206.9±9.9	**217.3±30.6**
Medium Replay	253.3±39.3	294.3±30.2	288.7±29.4	**357.2±67.2**
Medium	181.9±21.4	235.7±33.1	**343.7±32.7**	315.5±37.6
Medium Expert	213.8±57.4	274.2±28.5	440.9±21.8	**486.3±41.6**
Expert	277.7±51.7	358.2±21.5	470.6±21.2	**487.6±11.8**

To further show that DOM2 has the ability to generate high-quality actions with policy diversity, we show the number of good policies (i.e., with eposide return higher than 400 in the standard environment) found by the policies in evaluation in Table 8. The results show that under different datasets, DOM2 is able to find more diverse policies than existing algorithms.

Table 8: Comparison of the numbers of good policies found (policies with episode return of the trajectory larger than 400 in the standard environment) in the 3-Agent 6-Landmark environment.

Dataset	MA-CQL	OMAR	MA-SfBC	DOM2
Random	0.4±0.5	0.8±0.4	0.0±0.0	**12.8±3.4**
Random Medium	0.4±0.8	0.6±0.8	0.0±0.0	**9.2±1.6**
Medium Replay	0.2±0.4	0.4±0.5	4.4±2.8	**14.6±2.8**
Medium	0.4±0.5	0.4±0.8	9.6±1.9	**13.0±2.1**
Medium Expert	0.6±0.8	5.2±3.6	11.6±1.6	**19.2±1.2**
Expert	3.8±1.9	8.4±2.6	17.2±0.8	**20.0±0.0**

In spite of the statistical results shown in Table 8, we also visualize the trajectories generated by different algorithms, shown in Figure 9. We rollout the policy trained by different algorithms for 5 times under the same initialized position. The trajectories are colored red, blue, and purple to represent that they are generated by 3 different agents. The green dots are the landmarks. The task for the agents is to reach 3 green landmarks without collision. Different strategies in different background colors mean that 3 agents reach the landmarks and complete the task in various ways. The visualization results show that by multiple attempts, DOM2 finds 5 strategies, however, the numbers of strategies found by MA-CQL, OMAR and MA-SfBC are 2, 2 and 3, respectively. It shows that the policy trained by the DOM2 algorithm possesses high diversity, in other words, DOM2 is capable of generating more diverse policies.

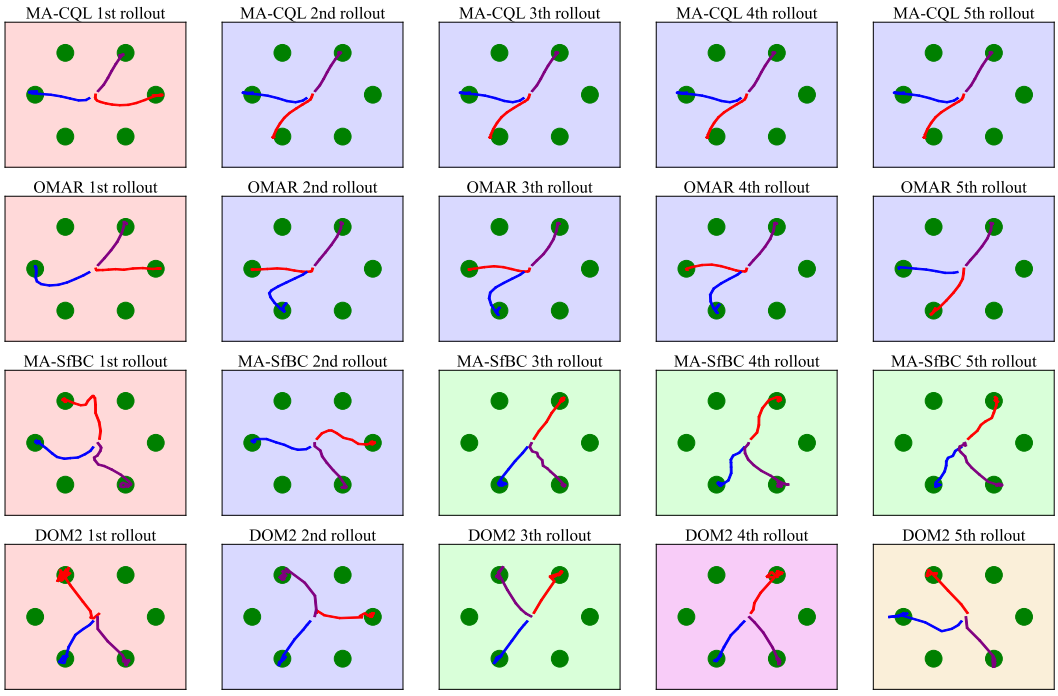

Figure 9: Visualization of trajectories generated by different algorithms with the same initialized position (the center of space) for the 3-agent 6-landmark setting. The red, blue and purple lines are trajectories of the three agents, and all landmarks are colored green. We use different background colors to denote different strategies (i.e., ways to reach three landmarks and complete the tasks) found by the algorithms. We notice that DOM2 finds 5 strategies, while the numbers of strategies found by MA-CQL, OMAR and MA-SfBC are 2, 2 and 3, respectively.

In Figure 10 (same as Figure 2), we show the average mean value and the standard deviation value of different datasets in the standard environment as the diagram (a) and in the shifted environment with 10-times evaluation in each episode as the diagram (b). The diagram (c) is the averaged number

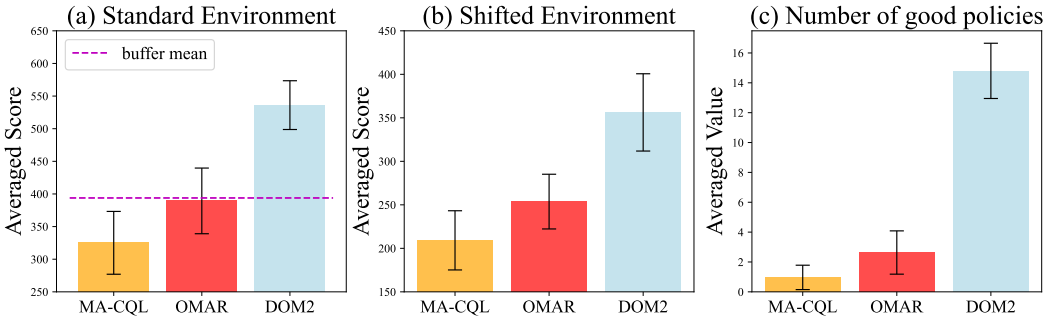

Figure 10: Algorithm performance in 3-Agent 6-Landmark examples among all kinds of datasets. (a): The averaged mean episode returns in the standard environment. (b): The averaged mean episode returns in the shifted environment. (c): Number of good policies (the episode return of the policy more than 400) found in the standard environment.

of good policies (the eposide return is higher than 400 in the standard environment) under different datasets. The performance of DOM2 is shown in the light blue bar. Compared to the MA-CQL as the orange bar and OMAR as the red bar, DOM2 achieves a better average performance in both settings, which means that DOM2 learns policies with much better expressiveness and diversity.

C.5 Ablation Study: Parameter Sensitivity

The effect of the regularization coefficient η Figure 11 shows the averaged mean episode returns of DOM2 over the MPE world task with different values of the regularization coefficient $\eta \in [0.1, 100.0]$ in 6 datasets. In order to perform the advantage of the diffusion-based policy, the appropriate coefficient value η needs to balance the two regularization terms appropriately, which is influenced by the performance of the dataset. For the expert dataset, η tends to be small, and in other datasets, η tends to be relatively larger. The reason that small η performs well in the expert dataset is that with data from well-trained strategies, getting close to the behavior policy is sufficient for training a policy without policy improvement.

The effect of the diffusion step N Figure 12 shows the averaged mean episode returns of DOM2 over the MPE world task with different values of the diffusion step $N \in [1, 10]$ under each dataset. The numbers of optimal diffusion steps vary with the dataset. We also observe that $N = 5$ is a good choice for both efficiency of diffusion-based action generation and the performance of the obtained policy in MPE.

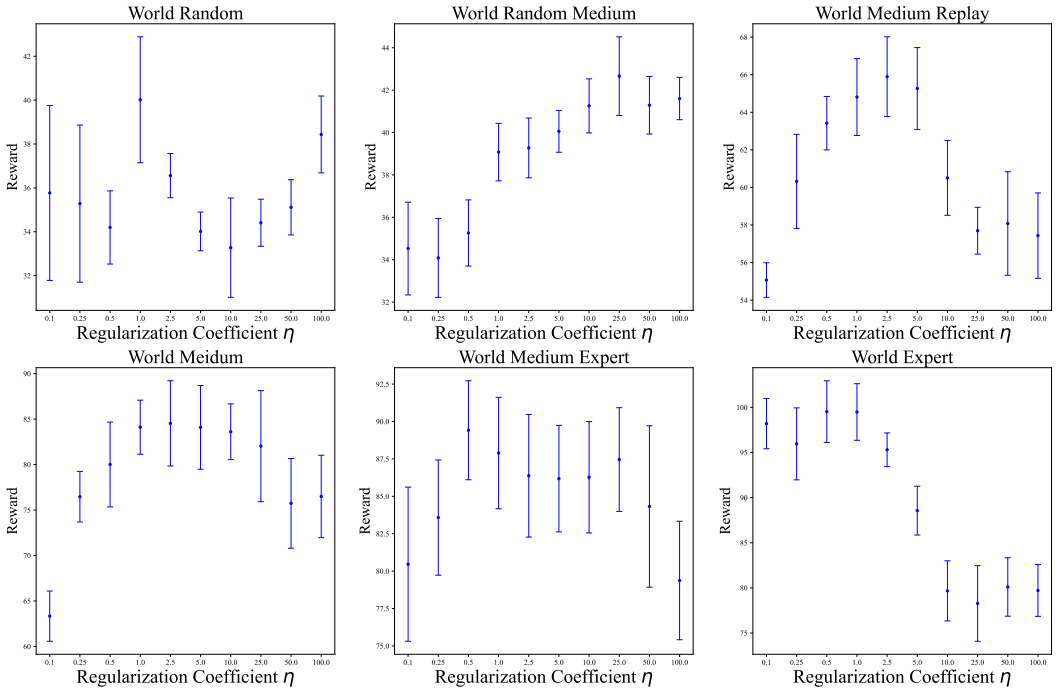

Figure 11: The effect of the η value in MPE World in 6 different datasets.

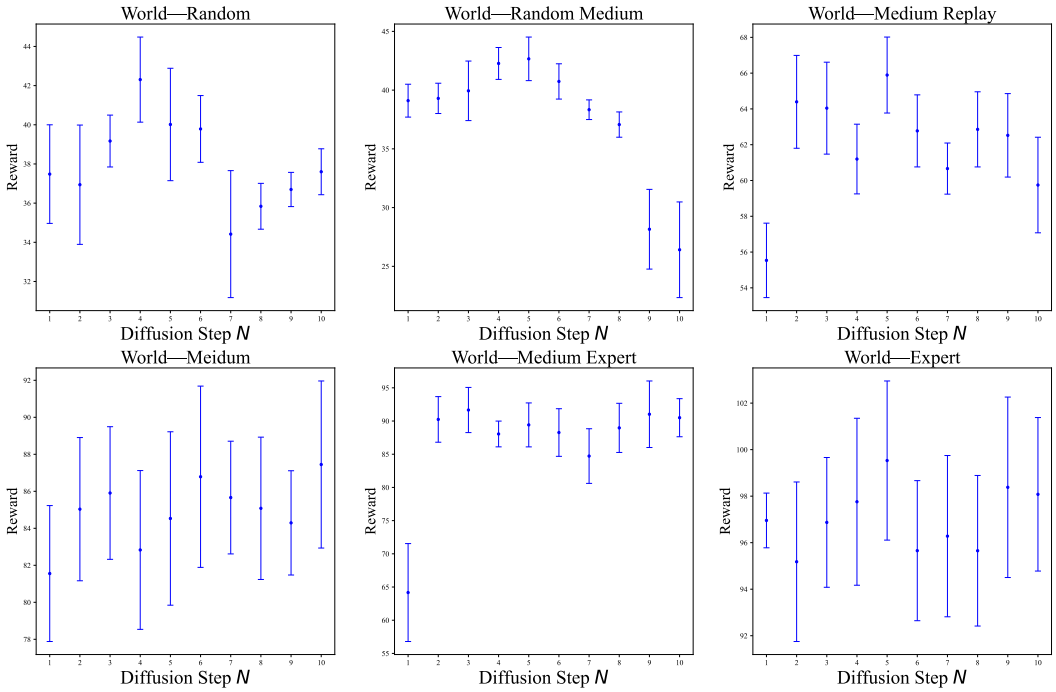

Figure 12: The effect of the diffusion step N in MPE World in 6 different datasets.